PSEUDO 3-D IMAGERY OF THE STATE LINE FAULT SYSTEM

STEWART VALLEY, NEVADA

USING SEISMIC REFLECTION DATA

By

Sandra C. Saldaña

Bachelor of Science
University of Nevada, Las Vegas
2007

A thesis submitted in partial fulfillment
Of the requirements for the

Masters of Science Degree in Geophysics

Department of Earth and Environmental Science

Graduate College
New Mexico Institute of Mining and Technology
May 2009

ABSTRACT

Pseudo 3-D Imagery of the State Line Fault System
Stewart Valley, Nevada

By

Sandra C. Saldaña

Dr. Catherine M. Snelson, Examination Committee Chair
Assistant Professor of Geophysics
New Mexico Institute of Mining and Technology

The State Line fault system (SFS) is in the central Basin and Range province and may mark the eastern extent of the Eastern California Shear zone (ECSZ). The SFS consists of three main segments (from north to south): the Mesquite, Pahrump and Armargosa segments. Although the SFS has been found to have the potential of Mw 7+ earthquakes, little is known about the Quaternary history of the fault. We acquired high-resolution seismic reflection data in Stewart Valley, located ~50 km from Las Vegas, NV with the goal of using seismic reflection processing to produce a pseudo 3-D seismic cross-section of the SFS. During the summer of 2007 four seismic reflection profiles were acquired in Stewart Valley: two normal and two parallel to the mapped traces of the SFS. In addition, in 2008, a series of shorter higher-resolution seismic reflection profile were acquired over the fault location after review of the 2007 data. These data reveal subsurface stratigraphy that was used to resolve the subsurface geometry of the SFS and estimate the Pleistocene slip rate. In Stewart Valley, the SFS exhibits a flower structure with a Pleistocene slip rate of 0.9 +6.5/-0.8 mm/yr, as estimated from an offset debris flow. The Pleistocene slip rate

estimate suggests that the slip rate along the SFS has slowed during the Quaternary, suggesting that dextral shear strain has migrated onto faults to the west of the SFS.

ACKNOWLEDGEMENTS

Many thanks to the Nevada Bureau of Land Management (BLM) and the private land owners who granted permission for the survey: Jacqueline and MC Spear, Christopher and Kellie Caracci, Ashraf Sarah Golshahi, Kenneth Newby, Myrwin and Dawn Anderson. Thanks to Cathy Wiley of the Public Lands Institute for her help with permitting. Thanks to the UNLV Applied Geophysics Center (AGC) for the use of the recording equipment and mini-vibroseis source. Thanks to my committee Drs. Catherine Snelson, Gary Axen, Sue Bilek and Wanda Taylor for their support through this process. Special thanks to Drs. Wanda Taylor and Gary Axen and Shelley Zaragoza for their infinite patience in teaching a physicist how to approach geologic problems. Thanks to Jonathon Carter for his time and insight with the well logs and interpretation. Funding for two summer internships was provided by IRIS. Thanks to Leigh Davidson and Barbara Fazio of EES for constant assistance. The following individuals provided field support under horrendously hot conditions: Matthew Beachly, Catherine M. Cox, Robert Davis, Michelle Stropky, Richard Phillips, Colin Robins, Chris Cothrun, Benjamin Dickenson, Wil and Emma Hyde and Jocelyn Padilla. Funding for this project was provided by the DOE funded Earthquakes in Southern Nevada (ESN) grants 85-6000411 and 08-65BB-00 as well Lawrence Livermore National Lab grant number B573241.

Eternal gratitude goes to Haha and Alley Cat for endless support and lots of truth serum. Appreciation goes to Sally Padilla for loyal support, undeniable logic and long walks. This manuscript benefited greatly from the humor of Betty and Bobby Gaines. Thanks go to Brad Christensen for his empathy and resilient belief

that it was possible. Gratitude goes to Hunter Knox and Alex Rinehart for being real. Many thanks to Javier and Cynthia Treviño for excellent advice over awesome salmon. Finally, it was Glenn and Anita Saldaña who taught me by example how to face adversity with courage and find my own way. This thesis is dedicated to my grandparents John Halvard and Thelma Erickson who will always live my memory.

TABLE OF CONTENTS

LIST OF FIGURES

LIST OF TABLES

This thesis is accepted on behalf of the
Faculty of the Institute by the following committee:

Advisor

Date

I release this document to the New Mexico Institute of Mining and Technology.

Student's Signature   Date

CHAPTER 1 INTRODUCTION

Geologic and geodetic investigations indicate that the San Andreas Fault (SAF) system accommodates most of the dextral shear between the North American and Pacific plates (Dokka and Travis, 1990; Savage et al., 1990). However, these same studies also estimate that ~25% of the strain is accommodated by the Eastern California Shear Zone (ECSZ) (Figure 1) (e.g., Bennett et al., 2003). The northern end of the ECSZ connects to Walker Lane (WL) while the Intermountain Seismic Belt (IMSB) lies to the east. Some workers suggest that the easternmost fault of the ECSZ is the State Line fault system (SFS) while others define the boundary farther east in Pahrump Valley, NV (Carter et al., 2008; Guest et al., 2007).

The State Line Fault System (SFS) is an ~200 km long right-lateral system that runs north-northwest from Mesquite to Amargosa, Nevada along the California-Nevada border (Figures 1 and 2) (e.g., Guest et al., 2007). The SFS is made of (from north to south) the Armargosa, Pahrump and Mesquite segments (Figures 1 and 2) (Guest et al., 2007). Most of the SFS runs through lacustrine or aeolian deposits that have not preserved the fault scarps well (e.g., Schweickert and Lahren, 1997; Snow and Wernicke, 2000). Paleo-seismic studies indicate that the SFS has ruptured at least once along the Amargosa segment and twice along the Pahrump segment during the Holocene, but little else is known about the Quaternary behavior the SFS (Anderson et al., 1995; Menges et al., 2003; Piety, 1996).

In addition, the SFS may pose a significant seismic hazard to the facility at Yucca Mountain as well as the cities of Las Vegas and Pahrump, Nevada. Based on its rupture length, the SFS has a potential for earthquakes of Mw 7+, but the large range in slip rate estimates makes it difficult to estimate the earthquake recurrence interval (e.g., Guest et al., 2007; Shields et al., 1998).   Geologic slip rate estimates for the SFS range from ~0.1- 2.3 mm/yr (Table 1) (Anderson, 1999; Guest et al., 2007; Louie et al., 1998; Wernicke et al., 2004). The slip rate proposed by Guest et al. (2007) of ~2.3 mm/yr is a magnitude greater then the slip rate used to determine the earthquake recurrence interval of >10 ka years (Menges et al., 2003). Insufficient data exists to estimate the earthquake recurrence interval based on the mid Miocene slip rate, however, if the mid Miocene rate is the current average for the system, then the recurrence interval would certainly be much less then the current estimate. Therefore, slip rate during the Quaternary is desirable in order to understand how the system is evolving and what potential exists for strong ground motion.

Geologic slip rate estimates for the SFS also disagree with the modern, geodetically derived slip rate of 1 mm/yr (Table 1) (Anderson, 1999; Guest et al., 2007; Louie et al., 1998; Wernicke et al., 2004). This relationship between the geologic and geodetic slip rates is unusual for the ECSZ, where the geodetic slip rates are generally higher than the geologic rates (e.g., Frankel et al., 2007; Hill and Blewitt, 2006). Guest et al. (2007) proposed four possibilities for the discrepancy between slip rates: 1) strain is being temporarily transferred to other fault systems to the west for some finite period; 2) strain is continuing to accumulate along the SFS but has not been released in any significant manner during the Holocene; 3) the faults making up the ECSZ formed sequentially from east to west and the strain once experienced by the SFS has now permanently migrated to younger fault systems farther west; or 4) the poor surface expression of the SFS has led to underestimated geologically derived slip rates.

Estimates of slip rate for the SFS during the Quaternary would give insight as to whether strain has been partitioned elsewhere in recent time and allow for inferences related to the earthquake recurrence interval for the system (e.g. Neimi et al., 2005). However, none of the estimated offsets, on which the slip rates are based, utilize Quaternary markers (Figure 2 and Table 1) (e.g., Guest et al., 2007). Therefore, knowledge of the slip rate during the Quaternary would be helpful in determining if strain has been partitioned west of the SFS to the Death Valley fault zone (e.g., Neimi et al., 2005). If strain has been partitioned from the SFS to the Death Valley fault zone, one would expect a decrease in the rate of offset along the SFS in recent time (e.g., Guest et al., 2007). A decrease in the rate of offset with time along the SFS would also indicate that the recurrence interval for events along the SFS is increasing with time, lessening the risk for strong ground motion to nearby cities (e.g., Guest et al., 2007).

The center portion of the SFS is comprised of the Pahrump Valley and Stewart Valley (SVF) faults, the latter is the focus of our study (Hoffard, 1991). In an effort to better constrain the history of slip along the SFS during the Quaternary and obtain information related to the subsurface structure of the system, we conducted a high-resolution pseudo 3-D seismic survey across the SVF, located ~50 km from the city of Las Vegas, NV (Figures 1-3).

Using our pseudo 3-D model of the SVF, we derived a slip rate of 0.9 +6.5/-0.8 mm/yr for this portion of the SFS based upon offset of an interpreted debris flow. This estimate indicates that strain has been partitioned away from the SFS over time which allows for a better understanding of the potential for strong ground motion in area.

Table 1. Slip Rate Data for SFS

Slip Rate Estimate	**Time Interval for Average**	**Offset Marker No. (Figure 2)**	**Offset (km)**	**Offset Marker/Kind of Estimate**	**Location**	**Comments**	**Reference**
2.3 ±0.35	13 - 0 Ma	2	~30	~13.1 ±0.02 Ma volcanic and rock avalanche deposits	Mesquite segment (Figure 2)		Guest et al., 2007
0.9 mm/yr	Modern			Geodetically Derived	Amargosa Segment SFS, Near Yucca Mountain (Figure 2)	Modeled with locking depth at 12 km	Wernicke et al., 2004
		3	10-20	Correlated pre-Cenozoic faults and facies trends	Pahrump Segement (Figure 2)		Burchfiel et al. (1983); R. L. Christiansen, personal communication in Stewart et al. (1968)
<0.2 mm/yr	Quaternary			Based on weak scarp morphology along Pahrump Segment	Pahrump Segement (Figure 2)	Basis for estimate may be invalid for faults with dominately lateral motion	Anderson, 1999
>0.1 mm/yr	Holocene		0.018	Shallow 3-D seismic utilizing offset spring mound	Southern Stewart Valley	Shallow seismic data used for estimate.	Louie et al., 1998
		1	3	Mesozoic faults and folds	Southern Mesquite Segment of SFS (Figure 2)		Walker et al., 1995

Summary of offset and slip rate data for the SFS. Lack of data from the Quaternary has made it difficult to assess the seimic hazard of the SFS.

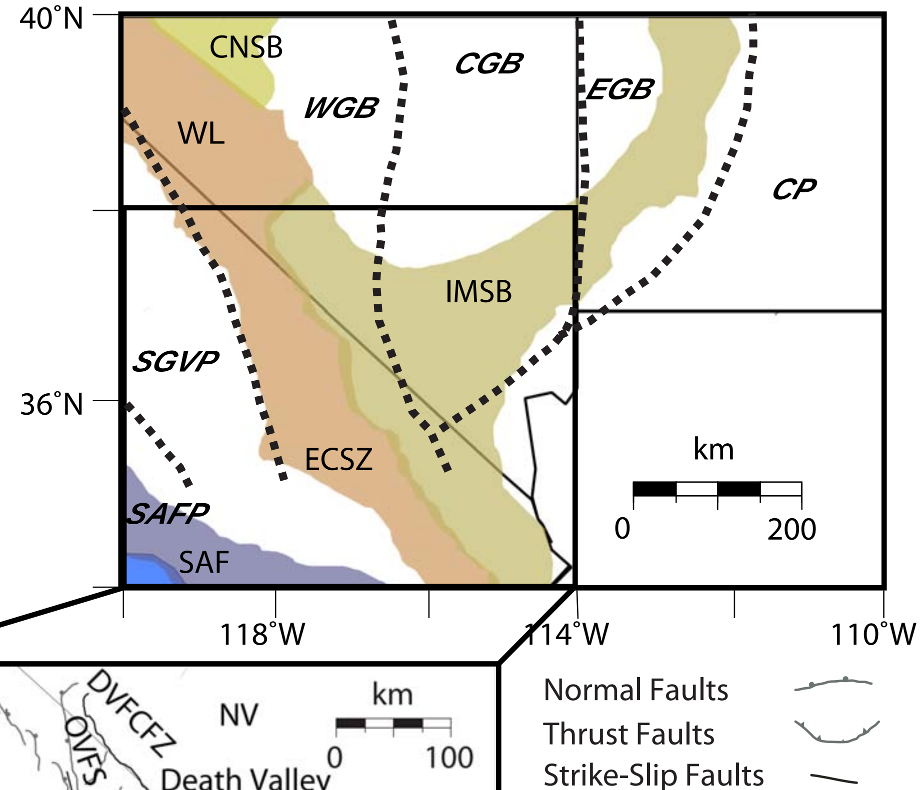

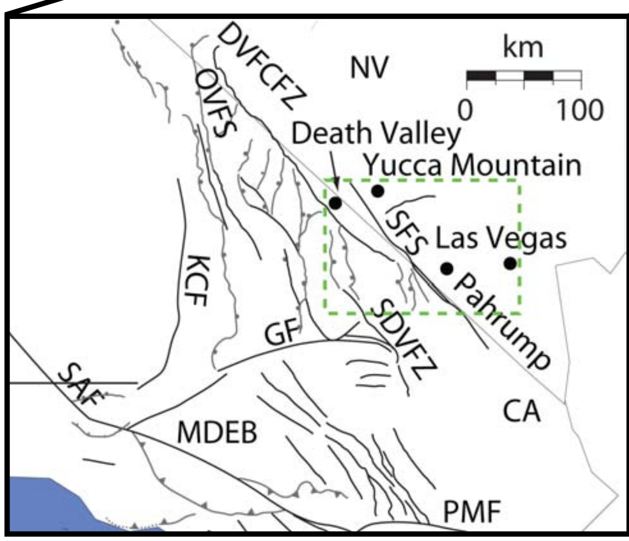

Figure 1.
(Top) Location of the Eastern California Shear Zone (ECSZ) (tan). Abbreviations: Walker Lane (WL), Intermountain Seismic Belt (IMSB) (dark yellow), San Andreas fault system (SAF) (purple), Central Nevada Seismic Belt (CNSB) (yellow) (Bennett et al., 1999; Oldow, 2003). Dashed lines indicate geodetic provinces (bold italic): SAFP-San Andreas Fault Province, SGVP-Sierra Nevada/Great Valley Province, WGB-Western Great Basin, CGB-Central Great Basin, EGB-Eastern Great Basin, CP-Colorado Plateau (Wernicke et al., 2004). (Bottom) Regional setting of the SFS. Green box indicates the location of Figure 2. The systems east of and including the Mojave Extensional Block (MDEB) are considered part of the ECSZ while the SFS forms the eastern limit of the ECSZ. The SFS is located along the western edge of the town of Pahrump and ~90 km from the city of Las Vegas, NV, (after Guest et al., 2007 and Dokka and Travis 1990). Abbreviations: SAF—San Andreas fault, PMF—Pinto Mountain fault, GF—Garlock fault, SDVFZ—Southern Death Valley fault zone, KCF—Kern Canyon fault, OVFS—Owens Valley fault system, DVFCFZ—Death Valley Furnace Creek fault zone, SFS—Stateline fault system, MDEB – Mojave Desert extensional block.

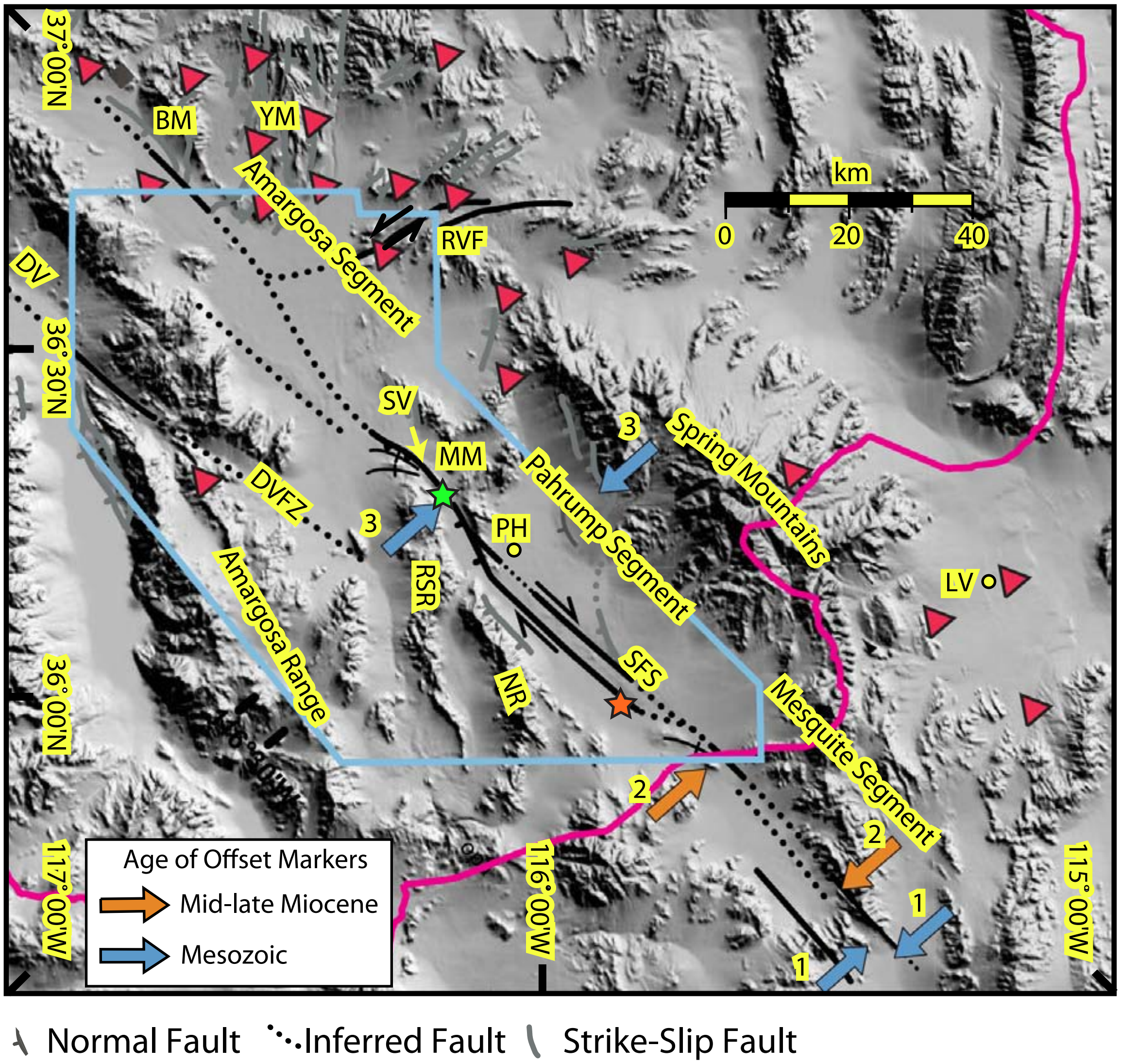

Figure 2. Regional setting for Stewart Valley. Green star shows the location of the seismic survey of Figure 3. Red Star is loction of previous geophyscal studies (Sheilds et al., 1998). Pink and blue lines indicate areas were gravity and magnetic data were collected (Blakely et al., 2000b). Red Triangles indicate the GPS locations of Wernicke et al., 2004. Colored arrows indicate age of offset markers numbered and referenced in the Table 2. Black arrows show the sense of movement along the Stateline fault system (SFS) and the Rock Valley Fault (RVF). Abbreviations: Bare Mountain (BM), Death Valley (DV), Death Valley fault zone (DVFZ), Las Vegas (LV), Montgomery Mountains (MM), Nopah Range (NR), Pahrump (PH), Resting Springs Range (RSR), Stewart Valley (SV), Yucca Mountain (YM) (after Guest et al., 2007). DOQ from USGS, 2009.

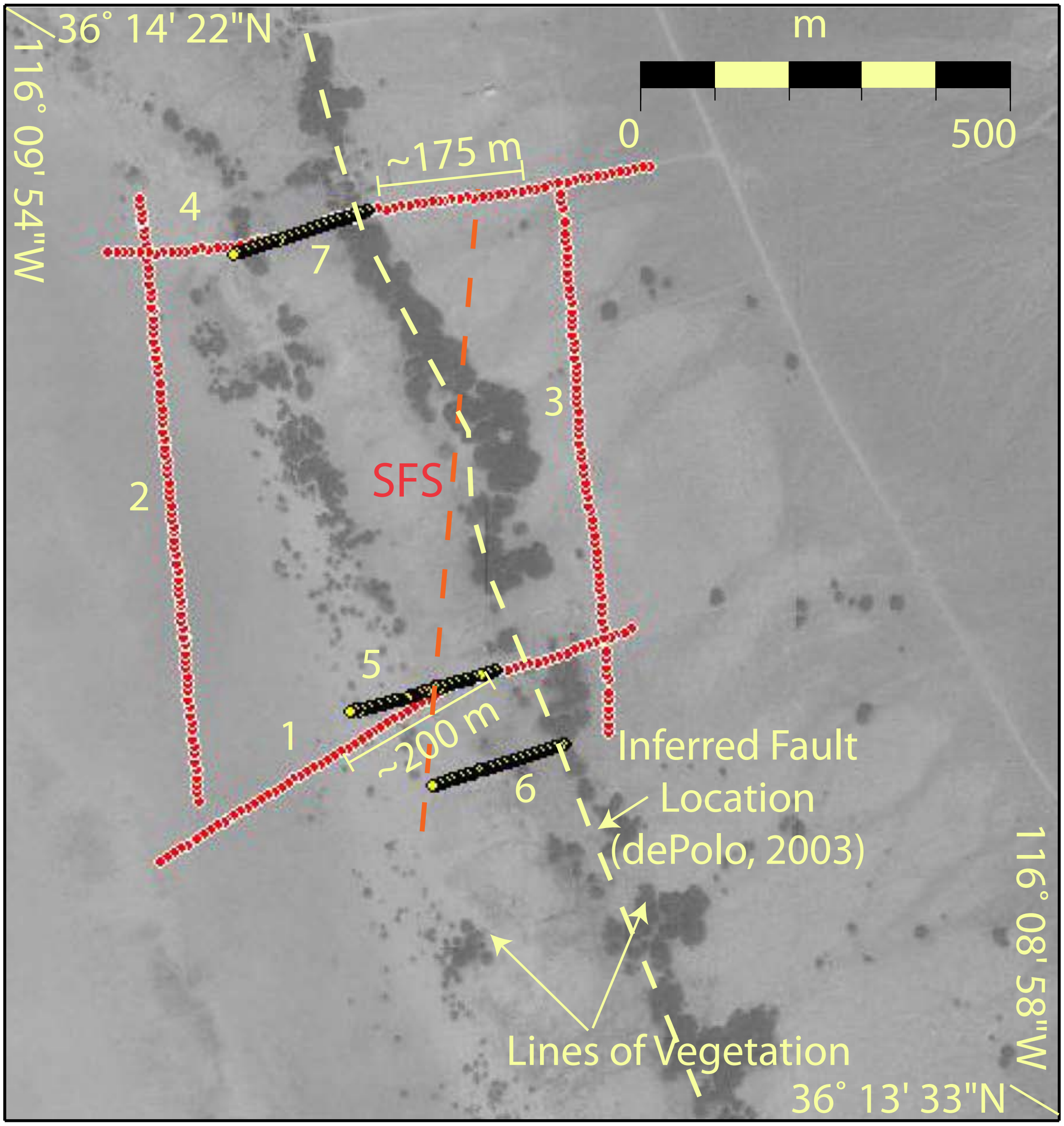

Figure 3. Map of the seismic reflection lines collected in 2007 and 2008. Digital Orthoquade (DOQ) (USGS seemless DEM) superimposed on the geologic map of de Polo (2003). Lines 1-4 (red dots) were collected at 10 meter source and 5 meter station spacing. Lined 5-7 (black & yellow dots) was acquired at 3 m station and receiver spacing. Extent of the SFS flower structure along lines 1 and 4 are indicated by the brackets. The SFS bears north (red dashed line) from line 1 and as the flower structure narrows by ~25 m. Additionally, the SFS is does not run between the two lines of vegetation as inferred (dePolo, 2003). Instead it runs down dip of the modern alluvial fan and beneath the mapped aeolian deposits. DOQ from USGS, 2009.

CHAPTER 2 GEOLOGIC SETTING

Two tectonic regimes have existed in the central Basin and Range during the Cenozoic and persist today: right-lateral dominant and extensional Basin and Range dynamics (e.g., Wernicke, 1992). During the Miocene (22-17 Ma), extension in the form of detachment faulting dominated the Mojave desert and led to the formation of the Mojave Desert Extensional Block (e.g., Dokka and Travis, 1990). Later, the Mojave fault block experienced deformation and rotation related to movement along the right-lateral SAF system (Figure 1) (Dokka and Travis, 1990).

The combination of the Mojave Desert extensional block and the Death Valley and Furnace Creek fault systems were originally grouped together into the Eastern California Shear Zone (ECSZ) (Figure 1) (e.g., Dokka and Travis, 1990). Although it is not well defined, the ECSZ has been mapped as far north as Owens Valley as well as extending to the Gulf of California and occupying a lateral zone of ~160 km from just east of the Sierra Nevada Front to include the SFS (Figure 1) (Dokka and Travis, 1990; Savage et al., 1990; Guest et al., 2007).

Geologically derived offsets from pre-Cenozoic markers for the three segments of the SFS are ~25-45 km for the Amargosa segment, 10 km to 15-19 km for the Pahrump segment and ~3 km for the Mesquite segment (Figure 2 and Table 1) (Stewart et al., 1968; Poole and Sandberg, 1977; Cooper et al., 1982; Burchfiel et al., 1983; Stevens, 1991; Walker et al., 1995; Schweickert and Lahren, 1997). Guest et al. (2007), found an offset of ~30 km along the Mesquite segment utilizing a mid-Miocene aged (13.1 ±0.02 Ma) marker.

CHAPTER 3 PREVIOUS GEOLOGIC AND GEOPHYSICAL STUDIES

A variety of geologic and geophysical studies have been conducted along the SFS to understand its location and subsurface geometry. These studies are outlined here to present context for our seismic results.

Potential Field Studies

Aeromagnetic data reveal the subsurface location of the SFS and indicate that it is continuous in the subsurface (Blakely et al., 2000). Based on gravity data, the SFS is interpreted as a wide zone (5-9 km) of west-stepping splays that cut into deep carbonate basement, indicating that the SFS has accommodated significant offset (Figure 2) (Blakely et al., 1998).

Shields et al. (1998) utilized ground-based magnetic and electromagnetic (EM) surveys to discern characteristics of the SFS in southern Pahrump Valley along three scarps. These data, in conjunction with the topographic data for each scarp, indicate that the western most scarp is the youngest (Figure 2) (Shields et al., 1998).

Controlled-Source Seismic Studies

Louie et al. (1998) used 3-D seismic reflection methods to find the near-surface offset (upper 73 m) of the SFS in southern Stewart and Pahrump valleys. The subsurface geometry of the SFS in both locations confirms that motion along the system is almost purely strike-slip (Louie et al., 1998). In addition, a minimum Holocene displacement of 18 m was determined implying a slip rate that is not less than 0.1 mm/yr (Table 1) (Louie et al., 1998).

Geodetic Studies

A dense GPS network was deployed from 1999-2003 to investigate the potential impact of faults close to Yucca Mountain (Figure 2 and Table 1) (Wernicke et al., 2004). Wernicke et al. (2004) modeled the Yucca Mountain GPS data using elastic models with a two-fault dislocation at depth. The model fit the data best when the SFS was included with the Death Valley fault system at a locking depth of 12 km. This dislocation model gives a modern slip rate of ~1 mm/yr for SFS (Wernicke et al., 2004).

Geologic Investigations

Several geologic investigations have been conducted along the SFS in order to deduce offset and slip rate for the system (e.g., Hoffard, 1991). Slip rate is particularly difficult to derive because the SFS has formed in depositional environments that have not preserved the scarps well and finding datable offset markers is problematic (e.g. Neimi et al., 2005). Offset markers used to estimate offsets along the SFS are all of pre-Quaternary age and give limited insight into the Quaternary evolution of the SFS (Figure 2 and Table 1)(Burchfiel et al., 1983; Guest et al., 2007; Stewart et al., 1968; Walker et al., 1995).

Guest et al. (2007) restored mid-Miocene volcanic deposits with their source locations and estimated 30 ±4 km of offset along the Mesquite segment, for a slip rate of 2.3 ±0.35 mm/yr (Guest et al., 2007). They noted the slip rate for the SFS since 13.1 ±0.02 Ma is 20 times greater then previous estimates derived from geologic observations (<0.2 mm/yr; Anderson, 2006) and is two to three times greater then the modern geodetic rate of ~1 mm/yr (Wernicke et al., 2004).

Carter et al., (2008) used well logs in Pahrump and Stewart valleys to infer the existence of a dextral system in Pahrump Valley that may actually define the easternmost fault of the ECSZ. However, well logs are too few and diffuse to make any inferences as to the recent offset along the SFS in Stewart Valley (Carter et al., 2008).

CHAPTER 4 SEISMIC DATA ACQUISITION AND PROCESSING

Seismic reflection data were acquired during the summers of 2007 and 2008. During the summer of 2007, we used a 144 channel Geode system with 4.5 Hz geophones to acquire four seismic lines, two parallel and two perpendicular to the inferred trace of the SFS in Stewart Valley (Figure 3). Each of the four lines were acquired at 10 m source and 5 m station spacing and varied in length from 550 to 715 m.

In 2008, the data collected during the previous year were used to constrain the location of the SFS and design a survey with a smaller tuning thickness. This knowledge allowed for the redesign and re-acquisition of a portion of lines 1 and 4 in addition to another line to the south of Line 1 in order to improve resolution over the SFS (Figure 3). The source and receiver spacing for these lines was 3 m with a total line length of 213 m. However, only Line 5, acquired over Line 1, ended up being useful in capturing the SFS, the other two lines missed the fault due to a lack of knowledge of the direction of strike and a problem with the GPS units (the common midpoint stacks for lines 6 and 7 are presented in Appendix A).

We used a T7000 mini-vibroseis source to acquire the Stewart Valley data (Table 2). For both acquisitions a linear 8 s sweep of 20-160 Hz was chosen to capture both the shallow high frequency response and the lower frequency response at depth. In addition, we acquired three sweeps at each source location to improve the signal-to-noise ratio.

These data were processed using Seismic Processing Workshop (SPW) and ProMAX. Seismic reflection data processing for the data presented here are outlined in Table 3. The initial velocity range for the constant velocity stacking was based on the first arrivals and velocities were improved from there based on the coherence of the reflectors. Velocity tables and the corresponding depth calculations are located in the Appendix B. The CMP stacks for each line are presented in Figures 4-8.

Our resulting 2-D seismic sections with clear, laterally consistent reflectors. Line 5, which was designed to maximize resolution, returned the best results. Multiple reflectors are visible where only a single reflector shows up on Line 1, acquired with less resolution (Figure 8).

We use these 2-D lines to produce a fence diagram of the area, with the tie points of the diagram occurring at intersection points in the 2-D data (Figure 9). At the corners of the cube the tie lines are projected because the deeper reflectors do not contain sufficient fold at the edges of the profiles to reach the ends of the cube. However, all the projected tie lines for the Stewart Valley data show good continuity of reflectors, including the intersection of lines 1 and 2, which do not intersect at the surface (Figure 3). This good continuity between two disconnected seismic lines is due to the laterally consistent lithologies at depth.

A comparison of the CMP stacks of lines 2 and 3 reveals a difference in reflector depths and amplitudes. The well logs compiled by Carter et al. (2008) indicate that the playa deposits of Line 2 are much more indurated and are found to have a slightly greater velocity than the dominantly aeolian deposits of Line 3. Investigation of the well logs in the area reveal interfingering of playa and aeolian deposits along the eastern edges of lines 1 and 4, collected normal to the trace of the

SFS (Figure 10).

Table 2. Acquisition Parameters.

Description	**Parameters**
File Format	SEG-2
Receiver Spacing	5 - Red Lines
	3 - Yellow Line
Source Spacing	3 - Yellow Line
	10 - Red Line
Geophones	4.5 Hz/Vertical
Pilot Signal	Synthetic
Vibroseis Sweep	Linear
	8 s
	20-160 Hz
Record Length	11 s
Sample Interval	Lines 2-4: 0.5 ms
	Lines 1 & 5: 1 ms
Assigned Pilot Channel	24

Table 3. Seismic Reflection Data Processing Flow

Processing Step	**Description**	**Software Used**
Data Input	SEG-2 binary data converted to SPW format	SPW
Vibroseis Correlation	Produces shot gathers from vibroseis data	SPW
Shot Gather Stacking	Stack multiple shots acquired at each shot point to reduce noise	ProMAX
Geometry	Apply geometry acquired with a Trimble GPS system	ProMAX
Trace Editing	Eliminate noisy traces	ProMAX
Top Muting	Eliminate refractions and traces that are noisy at higher frequecies	ProMAX
Bottom Muting	Eliminate surface wave energy	ProMAX
Velocity Analysis	Iterative constant velocity stacking to improve coherence of reflectors	ProMAX
Normal Moveout	Applied based on best velocities	ProMAX
CMP Stacking	Common mid-point summation	ProMAX

Figure 4. Uninterpreted (top) and interpreted (bottom) unmigrated CMP Stacks for Line 1, the southern-most east-west trending line. Where lines 1 and 5 overlap is shown. This line is 550 m long with a source spacing of 10 m and a receiver spacing of 5 m. Green arrow shows the location of onlap. Red arrow shows the location of air wave energy that did not stack out of the data due to its being located at the edge of the stack.

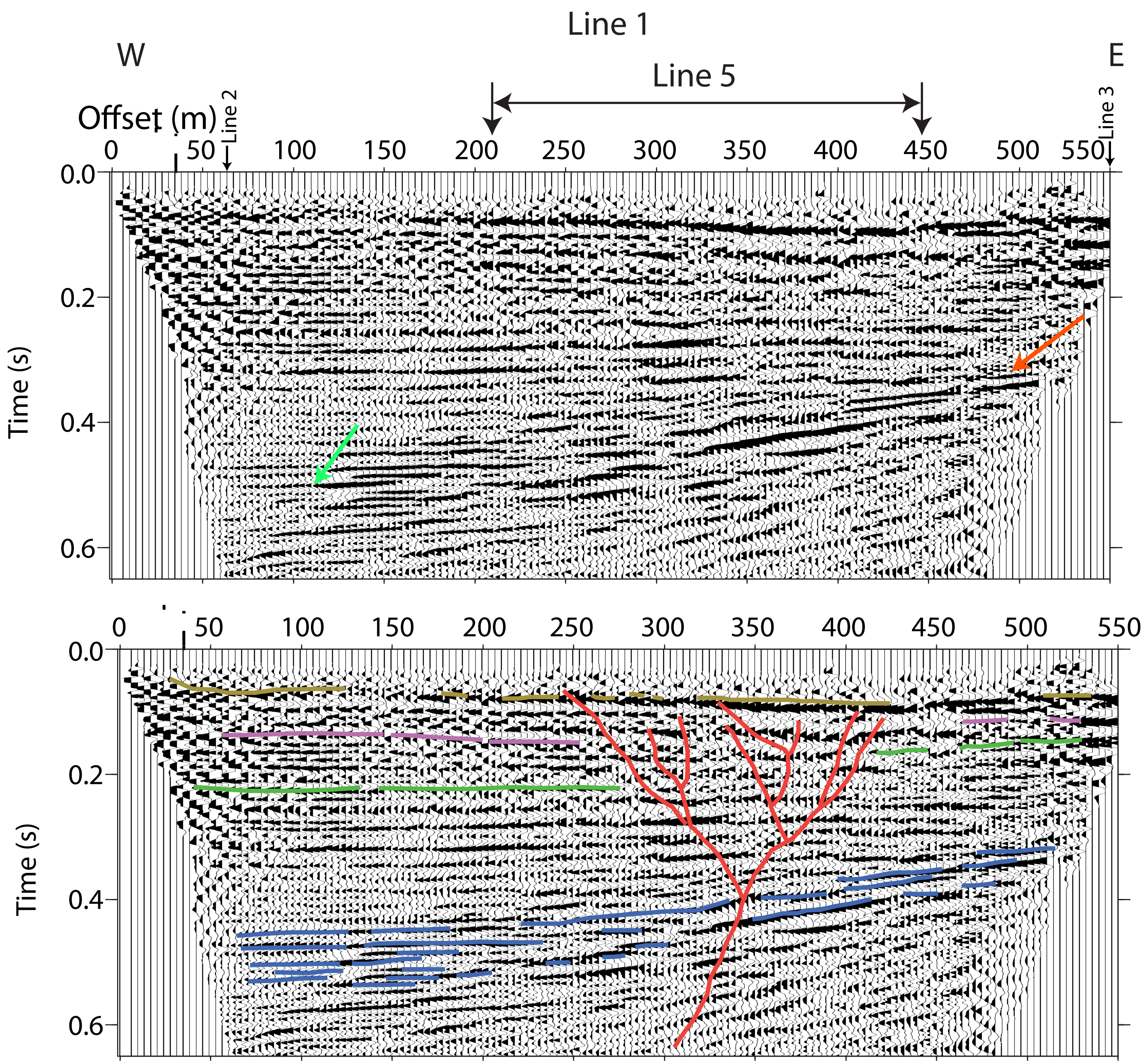

Figure 5. Interpreted (top) and uninterpreted (bottom) unmigrated CMP stacks for Line 2, the western-most north-south trending line. This line is 715 m long with 10 m source and 5 m station spacing. This line was collected over lacustrine deposits and exhibits a great deal of the laterally consistent layers as a consequence. In addition dipping reflectors are observed starting at ~0.45 s.

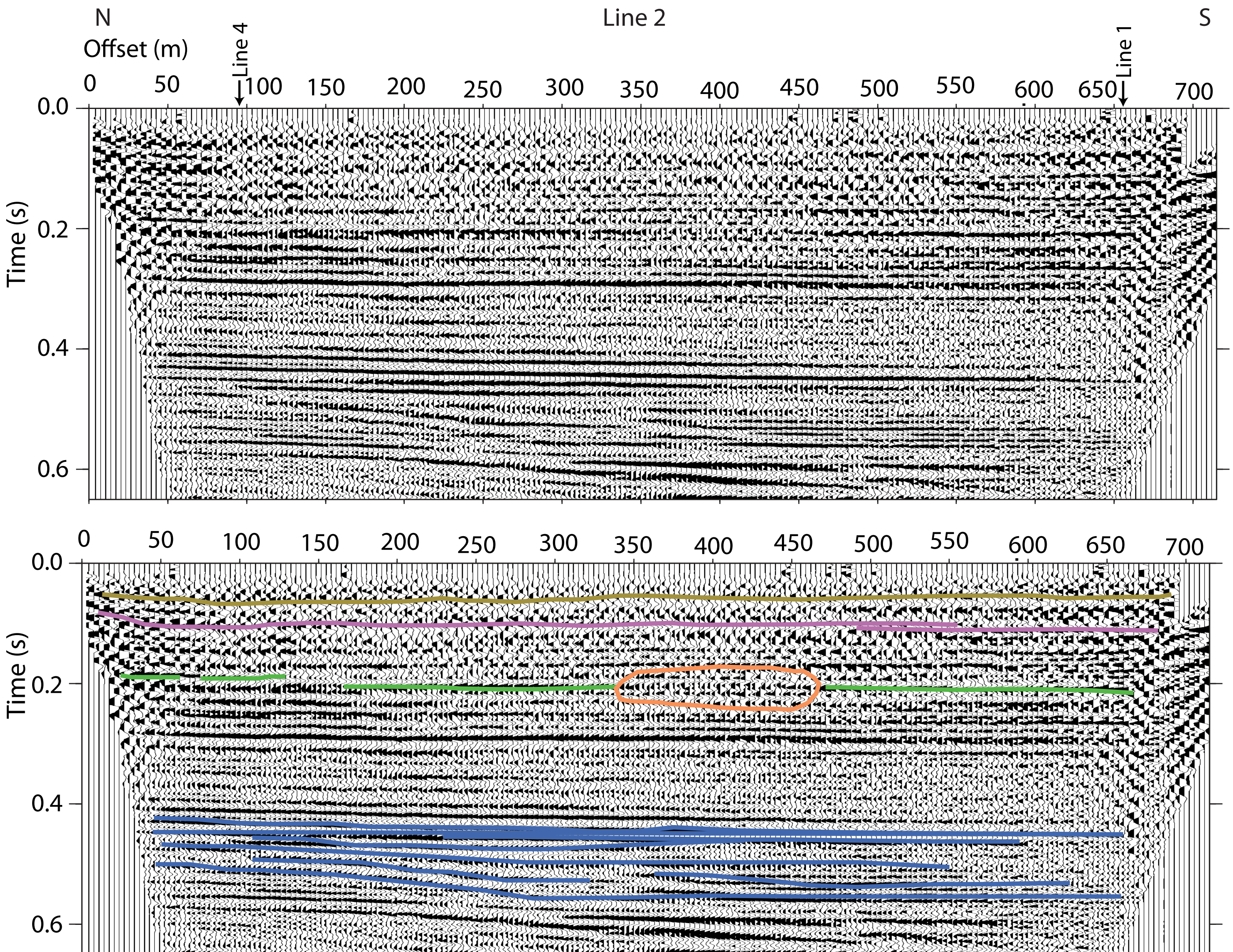

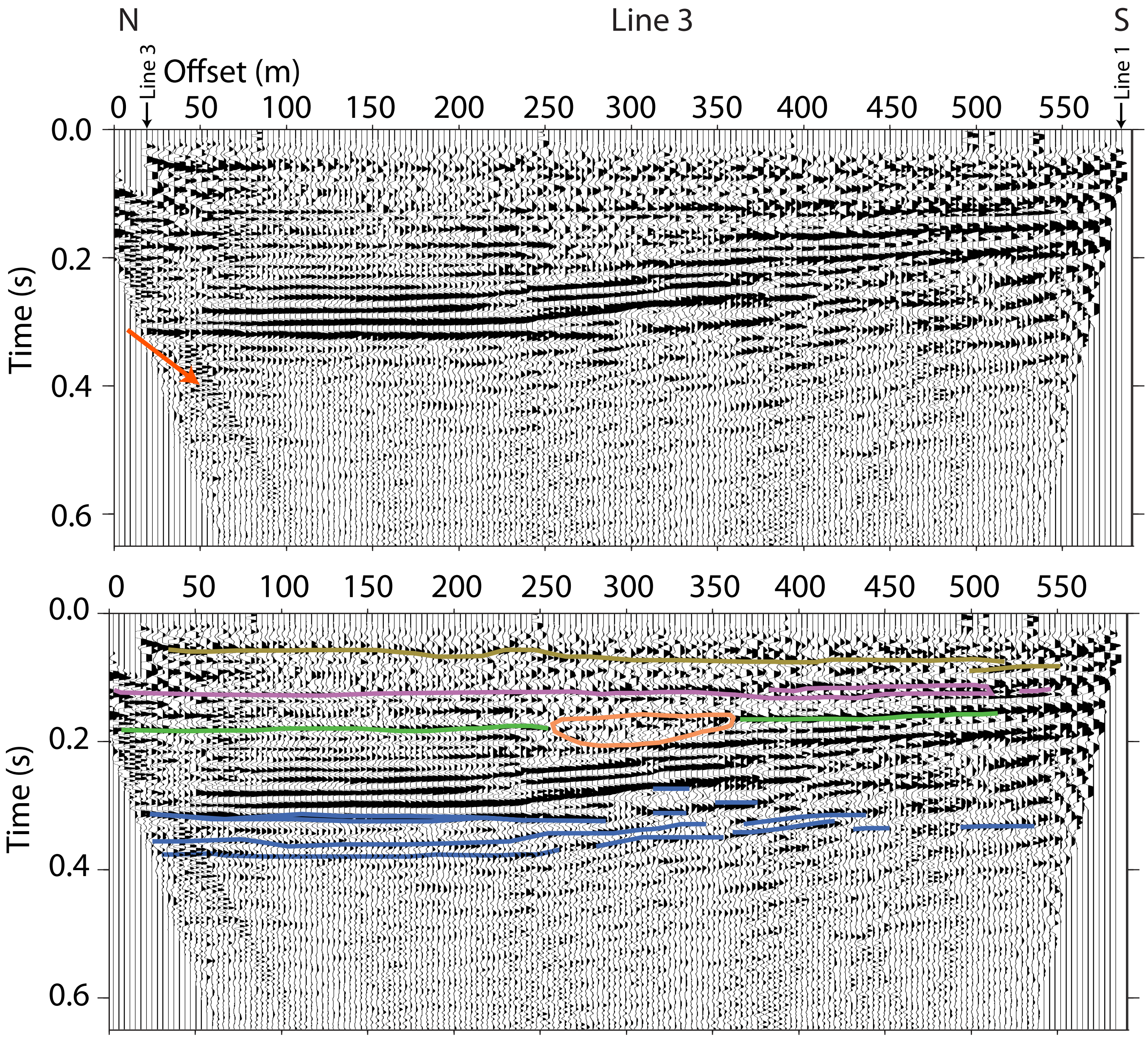

Figure 6. Uninterpreted (top) and interpreted unmigrated CMP stacks for line 3, the eastern-most north-south trending line. This line is 595 m long and was collected over interfingered aeolian and lacustrine deposits. This line also exhibits dipping beds which is consistent with its location as the closest line to the alluvial fan coming off the Montgomery Mountains to the east. Red arrow shows the location of an air wave that did not stack out due to its location at the edge of the stack.

Figure 7. Uninterpreted (top) and interpreted (bottom) unmigrated CMP StackS for Line 4, the northern-most east-west trending line and was 595 m long. Green arrow shows an example of onlap. Red arrow points to ariwave energy that was not eliminated during stacking due to being on the edge of the stack.

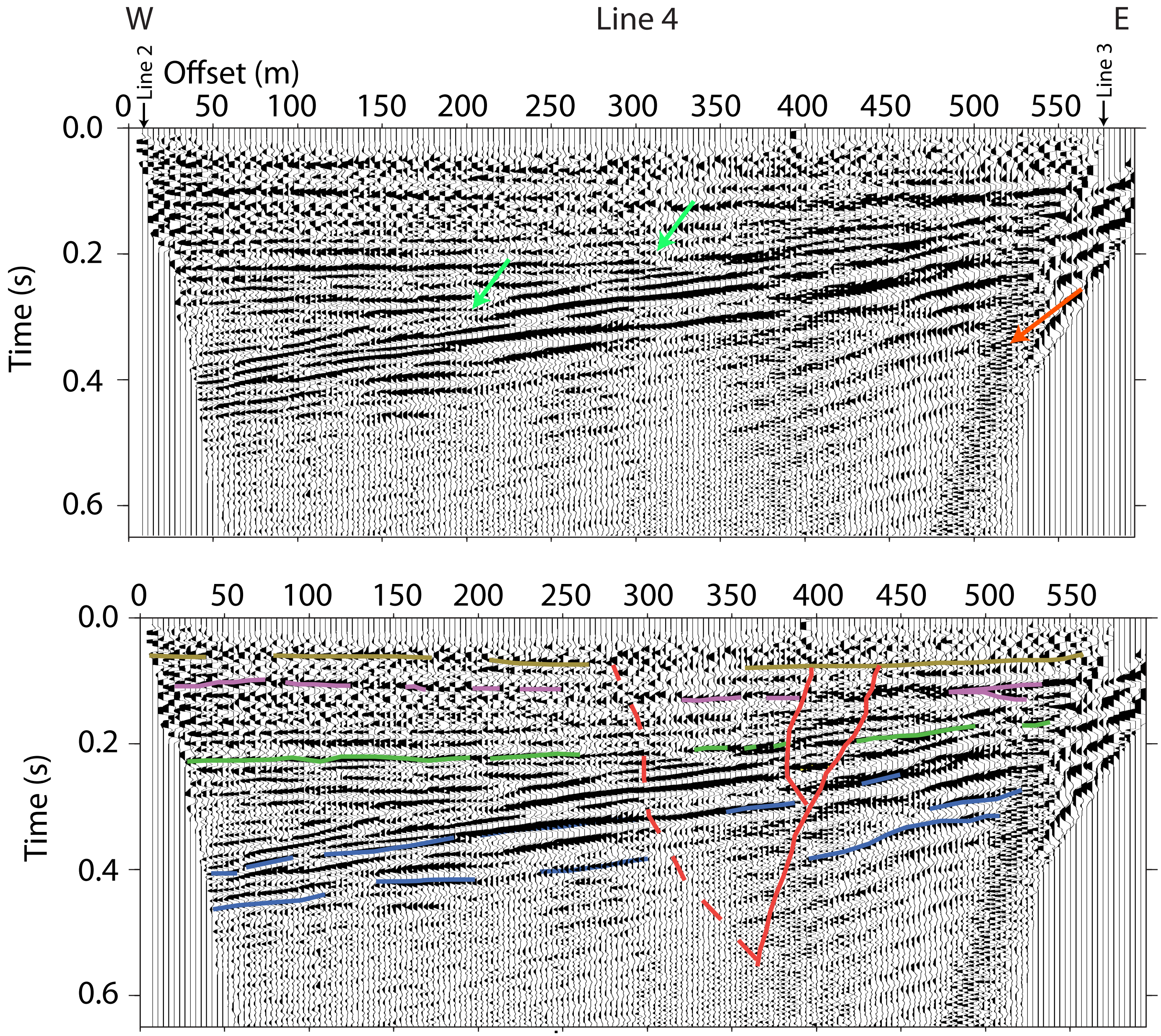

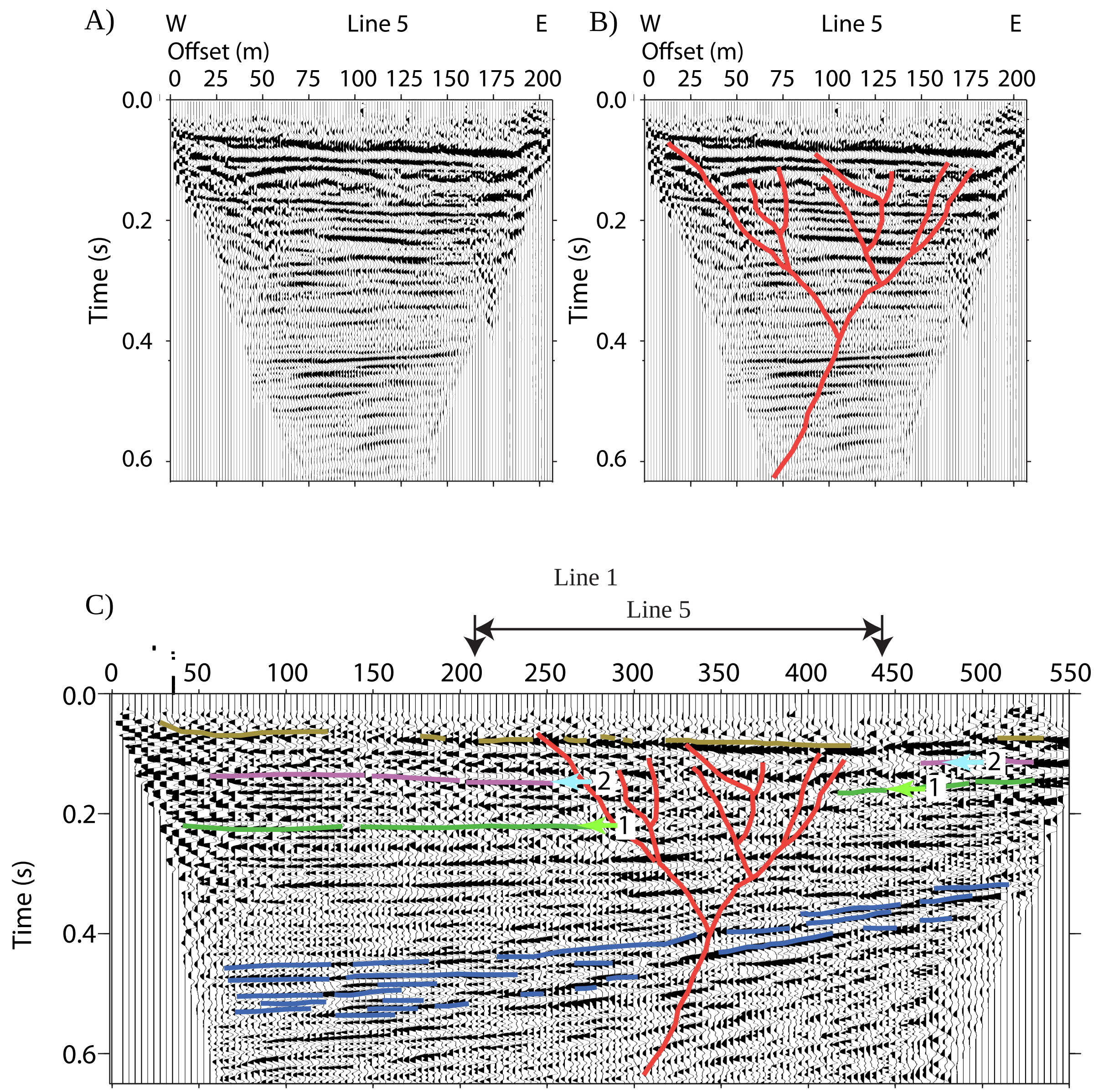

Figure 8. A) Uninterpreted unmigrated CMP stack for Line 5. This line is 213 m in length with source and receiver spacing at 3 m. B) Interpreted unmigrate d CMP stack for Line 5 C) Line 5 was acquired over part of Line 1 as shown. Due to the smaller station spacing, this line has more than twice the maximum fold of Line 1. Dark reflectors of Line 1 are split out into a few reflectors on line 5 due to the improved resolution. This line allows for the interpretation of the geometry of the SFS at depth. Green and blue arrows indicate dip-slip offset in the green and purple layers respectively. The green arrows are offset by ~27m while, the blue arrows are offset by ~65 m in the vertical.

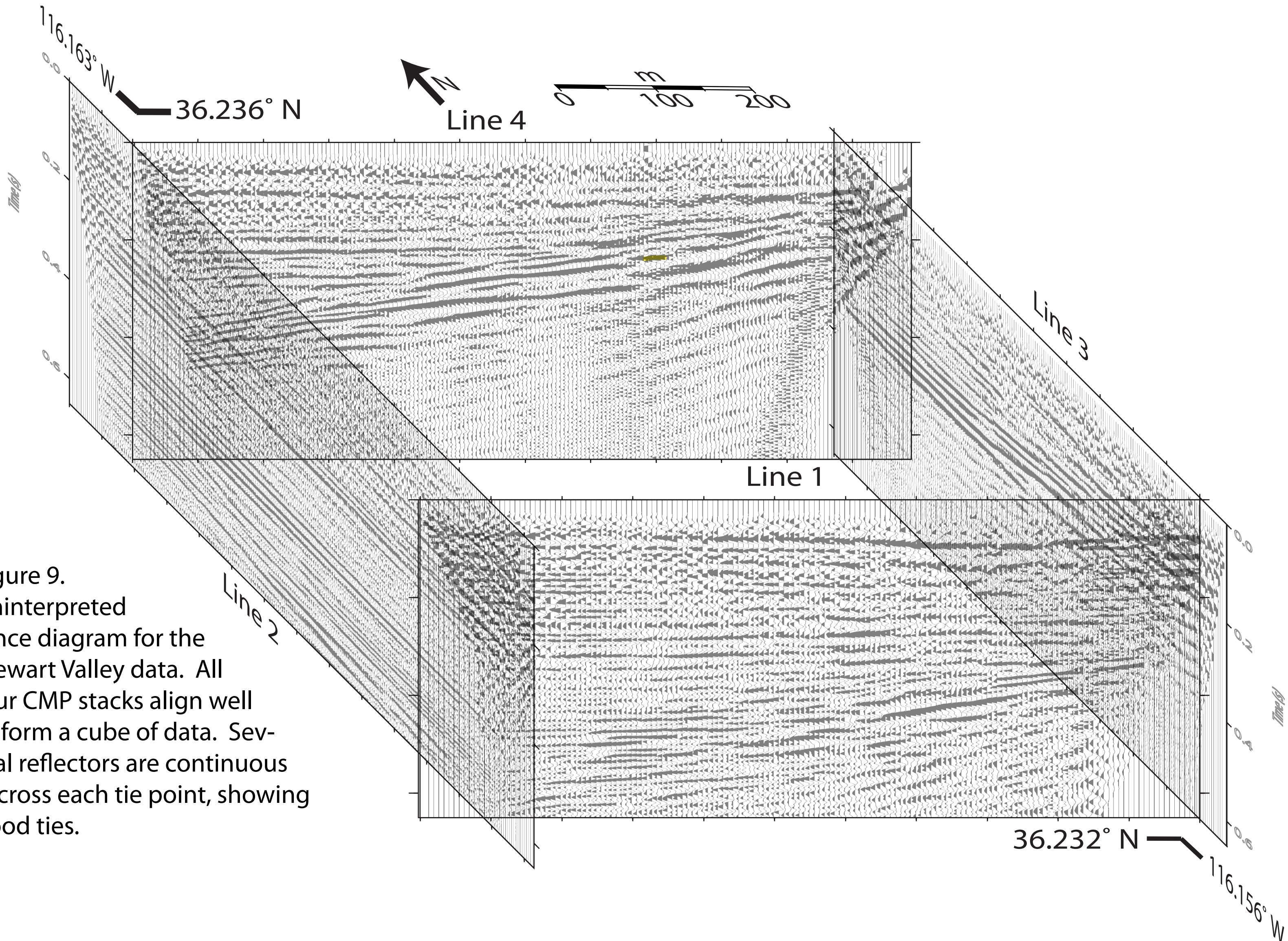

Figure 9.
Uninterpreted
fence diagram for the
Stewart Valley data. All
four CMP stacks align well
to form a cube of data. Sev-
eral reflectors are continuous
accross each tie point, showing
good ties.

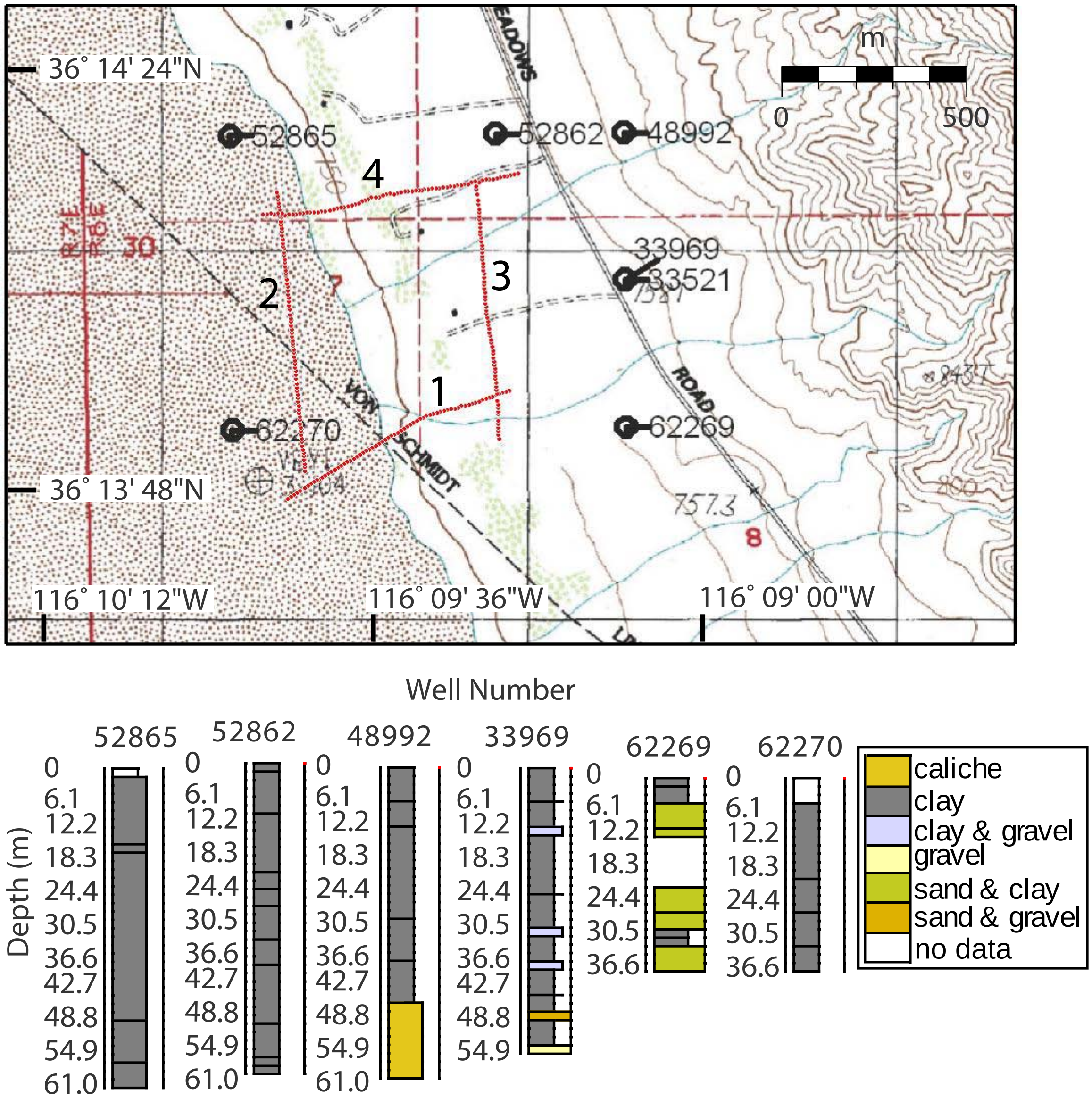

Figure 10. Well log data for the area were the seismic data was acquired. (Top) Locations of wells in the area. Black dots indicate well locations. Red lines indicate the location of the seismic lines. (Bottom) Wells in 2-D. Interfingering of lacustrine and aeolian deposits is evident from well logs especially along Line 3. Notice that the wells located near Line 2 are dominated by clay deposits while the wells located near Line 3 exhibit clay, sand and shale. This transition from clay to sand and shale is indicative of interfingering of deposis from different depositional enviroments and correlate to what is observed in the seismic data (modified from Carter et al., 2008).

CHAPTER 5 INTERPRETATION

The clarity of the Stewart Valley data allow for the interpretation of four stratigraphic contacts that can be traced around the perimeter of the cube as well as the subsurface geometry and extent of the SFS. The vertical resolution of the data is ~5 m for lines 1-4, while that of Line 5 is ~3 m. The deepest reflectors for these data occur along Line 2 at ~0.65 seconds which gives the minimum thickness of sediments in Stewart Valley of ~500 m (Appendix B).

The reflectors marked in brown, purple, green and blue are interpreted to be stratigraphic contacts (Figure 11). Based on the well logs, the brown and purple contacts are interpreted to represent a lacustrine contacts at depth ranges of ~32-46 m and ~58-67 m respectively (Figures 10, 11 and Appendix B). Because the green contact shows a similar seismic character as the brown and purple contacts, it is also interpreted to be lacustrine at a depth of ~91-140 m (Appendix B). Due its dipping nature, the blue contact is interpreted to be a paleo-fan surface and that varies in depth from ~250-440 m. The stratigraphic packages represented by the reflectors between these contacts all show thinning and thickening at locations that correspond with changes from lacustrine to aeolian depositional environments in the well logs.

An oval-shaped area of low reflectivity (outlined in orange, Figure 11) shows up on both lines 2 and 3 at depths of ~132 and 123 m respectively and disrupts the interpreted green contact (Appendix B). The lack of coherent reflectors within the anomaly is indicative of the deposition of unlayered or lithologically monotonous material (e.g., Badley, 1985; e.g., Sheriff, 1975). This feature is interpreted as debris flow (Figure 11). The seismic character and thickness (~18-38 m) of the anomaly is consistent with a series of debris flows that moved unconsolidated material along existing channels and across the basin floor. Debris flows coming off of the Spring Mountain Range that transverse the basin floor are common in Stewart Valley (de Polo, 2003).

The location of the SFS is interpreted from truncated, pinched out or offset reflectors along lines 1 and 4 (e.g., Sheriff, 1975). At depth the SFS is multistranded and displays a flower structure, common for a strike-slip fault that has experienced multiple events though time and is confirmed from the interpreted data (Figure 11) (e.g., McCalpin, 1996). Line 5 shows a relatively complicated tulip structure, which indicates strike-slip plus extensional motion (Figures 8 and 11).

Dip-slip motion along the SFS in Stewart Valley is evident in the interpreted purple green contacts by offset reflectors along Line 5. The purple and green layers are interpreted to be offset by ~14 and 33 m respectively (Figure 8 and Appendix B). The CMP stack for lines 1 and 5 indicates that the SFS does not disrupt the near surface reflectors including the interpreted purple layer as much as it does the deeper reflectors. This may explain why the dip-slip offset of the purple contact is much less than that of the green.

Seismic profiles 1 and 4 also captured the width of the fault zone (Figures 3 and 11). The SFS is ~200 m wide and is located between the two lines of vegetation along Line 1 and ~175 m wide east of the lines of vegetation along Line 4. Thus, the SFS appears to strike nearly north in the area surveyed (Figures 3 and

11). The eastern line of vegetation may exist due to water traveling down from the SFS to the topographic low of the playa deposits.

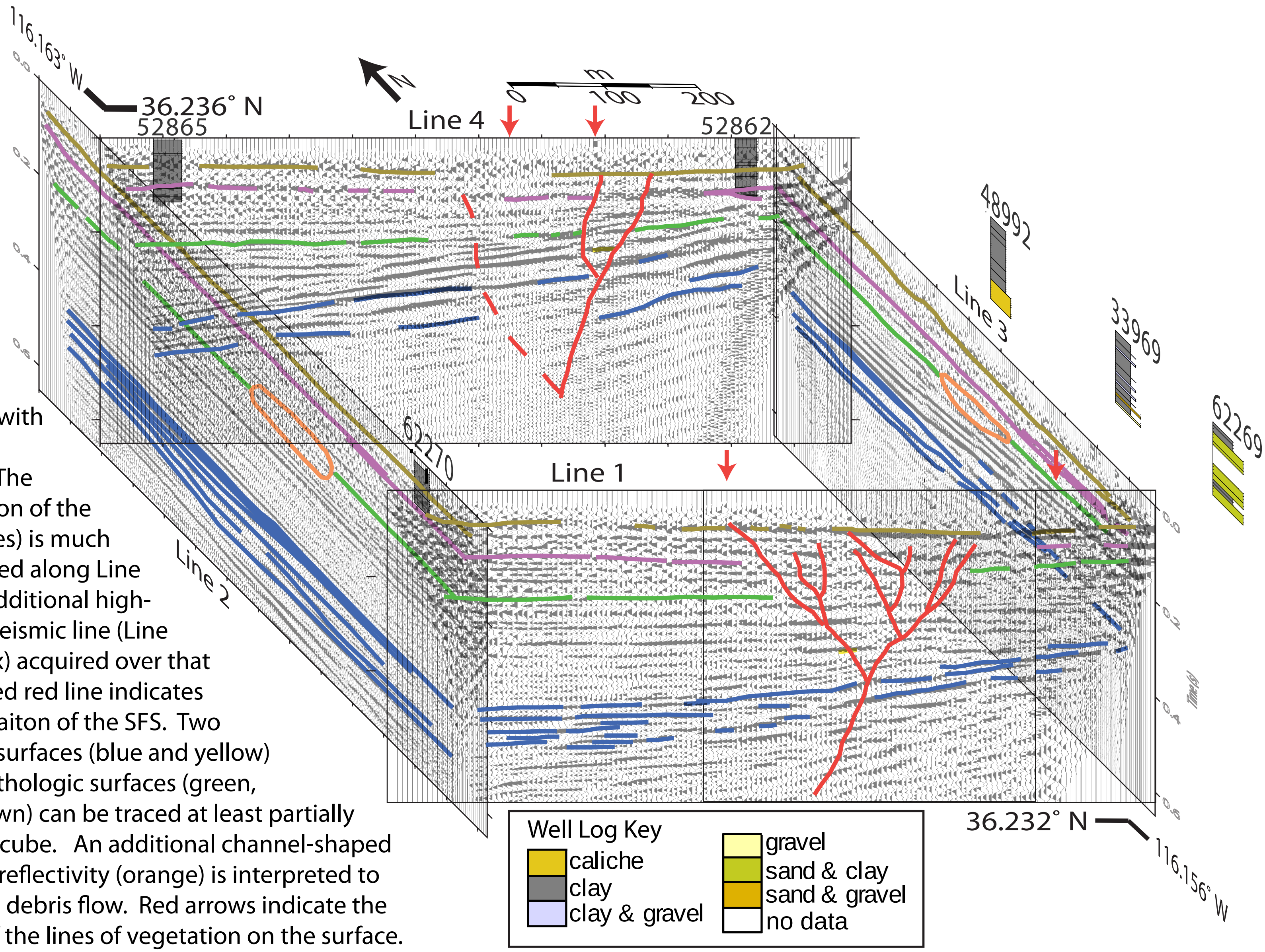

Figure 11. Interpreted fence diagram of the Stewart Valley data with well data projected. The interpretation of the SFS (red lines) is much more detailed along Line 1 due the additional high-resolution seismic line (Line 5- black box) acquired over that area. Dashed red line indicates inferred locaiton of the SFS. Two alluvial fan surfaces (blue and yellow) and three lithologic surfaces (green, purple, brown) can be traced at least partially around the cube. An additional channel-shaped area of low reflectivity (orange) is interpreted to be an offset debris flow. Red arrows indicate the locations of the lines of vegetation on the surface.

CHAPTER 6 SLIP RATE ESTIMATE

A Quaternary slip rate estimate may help resolve discrepancies in the geologic and geodetic slip rates and may lend insight into the earthquake hazard of the system (Table 1).

Because the original azimuth for the debris flow is unknown, we derived a range of offsets from the angles of stream channels coming off the alluvial fan surface directly to the east of the survey area. We then constrained the offset error based on seismic lines 1 and 4 and determine an offset of ~671 +264/-576 m (Figure 12). Lack of knowledge related to the strike of the fault zone contributes only ~5 m of error to the calculation for offset; therefore, most of the error in this calculation is derived from the angles of stream channels.

While age control is problematic in this area, general rates for sedimentation indicate the age of the offset debris flow is older than Holocene. Work conducted in the Tecopa basin, located ~43 km southwest of Stewart Valley, gives a range of sedimentation rates of 0.005-0.1 mm/yr (Morrison, 1991). Considering the interpreted debris flow varies in depth from ~132 m along Line 2 and ~123 m along Line 3, an age range of ~1.2-26 Ma is derived by dividing the depths by the assumed sedimentation rate. If the green contact is lacustrine, then its age is constrained by geologic mapping in the area, which gives the oldest lacustrine deposit an age of Pleistocene (de Polo, 2003). Using Pleistocene ages ranging from 0.126 – 1.806 Ma, a slip rate of 0.9 +6.5/-0.8 mm/yr is derived.

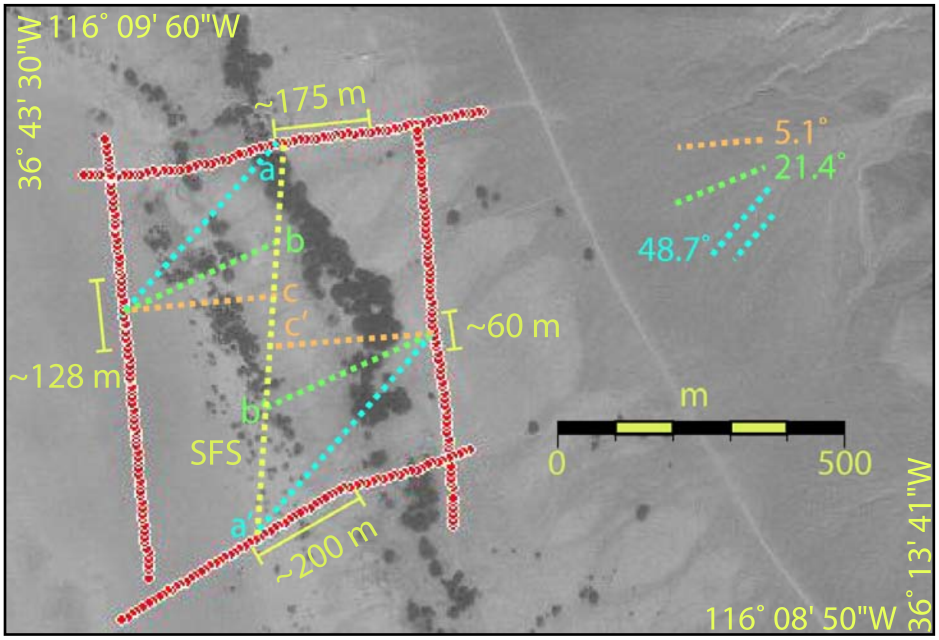

a-a′ ~680 m b-b′ ~283 m c-c′ ~85 m

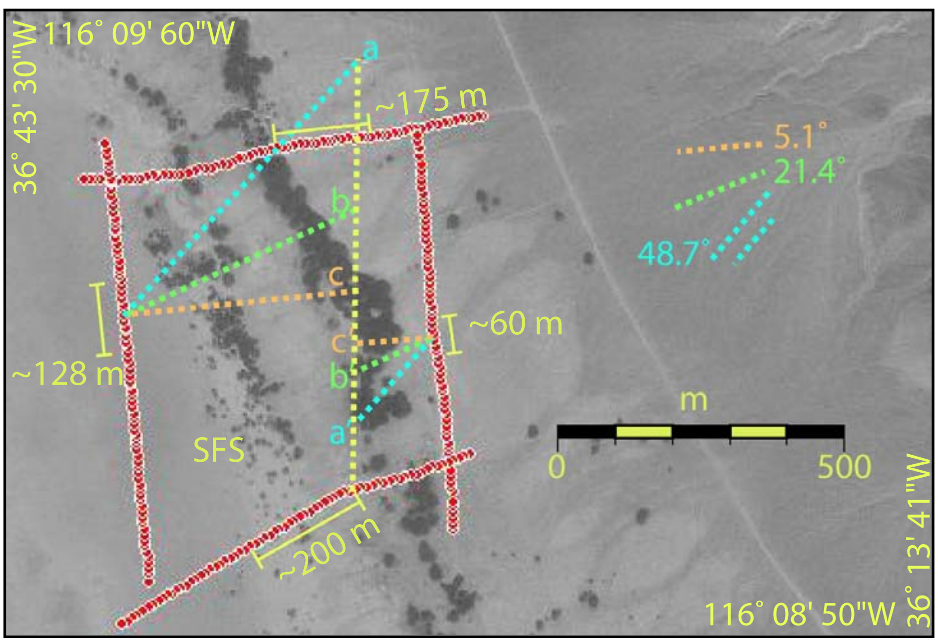

a-a′ ~632 m b-b′ ~290 m c-c′ ~90 m

Figure 12. Illustration of how the offset was derived for the debris flow. North and south brackets indicate the damage zone of the SFS as in Figure 11. East and west brackets show the extent of the interpreted debris flow in the subsurface. The orange, green, blue black and pink lines distinguish the different angles of stream channels coming off the nearby alluvial fan. These angles were used in addition to the range of the strike of the fault zone in determining the range of offsets for the debris flow. The best guess for the angle at which the debris flow was deposited is 48.7˚ (blue) because this is the angle of the modern drainage. Dashed yellow line is the SFS at its western most extent (top) and its eastern most extent (bottom). Angles of flow are color coded and correspond to the transects as shown.

CHAPTER 7 DISCUSSION AND CONCLUSIONS

The slip rate for the SFS has been estimated from 0.1-2.3 mm/yr (Table 1) (Anderson, 2006; Guest et al., 2007; Louie et al., 1998). These rates are contrary to the modern geodetically derived slip rate of ~1 mm/yr (Bennett et al., 2003). This inconsistency in slip rates makes it difficult to evaluate the seismic hazard for the nearby city of Las Vegas and the town of Pahrump, Nevada.

In an effort to gain insight into the behavior of the SFS in recent time, seismic reflection data were collected in Stewart Valley, Nevada. An analysis of these data reveals the geometry and sense of displacement (transtensional, at least locally) of the SFS at depth, which is in agreement with previous workers (e.g., Blakely et al., 1998; Hoffard, 1991). The SFS has formed a flower structure at depth, which is indicative of strike-slip faults that have been active through time (e.g., McCalpin, 1996). In addition, a few geologic surfaces can be traced through the cube of the pseudo 3-D model and give insight into the age of what is interpreted to be an offset debris flow. Although the age of the interpreted debris flow is unknown, the depth at which it occurs is consistent with its being mid to late Pleistocene in age and gives a Quaternary slip rate of 0.9 +6.5/-0.8 mm/yr.

Our findings indicate that the slip rate along the SFS has decreased during the Quaternary. If slip has slowed since the Miocene the question of how strain has been partitioned remains. One possibility is that strain has migrated west since the mid-Miocene. Shields et al. (1998) analyzed three fault scarps of the SFS in Pahrump Valley, Nevada and determined that western-most scarp was the youngest (Figure 2). In addition, aeromagnetic data defines the SFS as being made up of western-stepping splays (Blakely et al., 2000). These findings in conjunction with the decrease in slip rate along the SFS may indicate that at least some strain has migrated west over time (Guest et al., 2007).

Slowing in slip from south to north along strike has been observed west along the Death Valley – Furnace Creek (DVFC) fault zone and has led some workers to hypothesize that the same extensional transfer zones that accommodated block rotation during the mid-Miocene and Pleistocene may also be playing a role today in the transfer of strain north to the faults of Walker Lane (Frankel et al., 2007; Oskin and Iriondo, 2004). Several normal faults exist between the SFS and the DVFC fault zones (Figure 1), perhaps strain has migrated west to this system before moving north to Walker Lane.

Alternatively, the discrepancy in slip rates for the SFS may not be a discrepancy at all, but may simply reflect artifacts of a young, evolving system (e.g., Kirby et al., 2008). Slip rates have been found to differ spatially along the strike of individual fault systems within the ECSZ (e.g., Frankel et al., 2007; Kirby et al., 2008). Perhaps the difference in the geodetic and geologic slip rates for SFS are a function of where the slip rate was measured as some workers have found a decrease in slip rate along strike and to the north of center along the Owens Valley and DVFC systems (Frankel et al., 2007; Kirby et al., 2008). Fault systems such as the Death Valley and Rock Valley systems may be adding or taking away strain from the SFS along strike, which would cause a spatial difference in slip rate (Figure 2).

In any case, more definitive slip rate estimates along the SFS of Quaternary age would be helpful in determining the most recent activity along the SFS (e.g. Neimi et al., 2005). Future work might include age control on multiple Quaternary-aged offset stream channels in Stewart Valley (Neimi et al., 2005). Moreover, the acquisition of two additional parallel seismic lines located on either side of and closer to the SFS, in the area of interpreted debris flow, would be invaluable in constraining the angle at which it was deposited and thus more accurately constraining its offset.

References

Anderson, R. E. (1999). *Complete Report for Frenchman Mountain fault (Class A) No. 1117*, http://gldims.cr.usgs.gov/webapps/cfusion/Sites/qfault/qf_web_disp.cfm?disp_cd=C&qfault_or=148&ims_cf_cd=cf

Anderson, R. E. (2006). *Quaternary Fault and Fold Database for the United States, Fault 1076 Pahrump Fault*, http//earthquakes.usgs.gov/regional/qfaults/

Anderson, R. E., Crone, A. J., Machette, M. N., Bradley, L. A., and Diehl, S. F. (1995). *Characterization of Quaternary and Suspected Quaternary Faults, Amargosa Area, Nevada and California*, U.S. Geological Survey, OFR 95-613

Badley, M. E. (1985). *Practical Seismic Interpretation*, Prentice-Hall Inc., Englewood Cliffs, 266.

Bennett, R. A., Wernicke, B. P., Niemi, N. A., Friendrich, A. M., and Davis, J. L. (2003). Contemporary Strain Rates in the Northern Basin and Range Province From GPS Data *Tectonics*, 2, **22**, 1008.

Blakely, R. C., Langenheim, V. E., Ponce, D. A., and Dixon, G. L. (2000). *Aeromagnetic Survey of the Armargosa Desert, Nevada and California: A Tool for Understanding Near-Surface Geology and Hydrology*, U.S. Geological Survey, OFR 00-188

Blakely, R. C., Morin, R. L., McKee, E. H., Schmidt, K. M., Langenheim, V. E., and Dixon, G. L. (1998). *Three-Dimensional Model of Paleozoic Basement Beneath Amargosa Desert and Pahrump Valley, California and Nevada:*

Implications for Tectonic Evolution and Water Resources, U.S. Geological Survey,

Burchfiel, B. C., Hamill, G. S., and Wilhelms, D. E. (1983). Structural Geology of the Montgomery Mountains and the Northern Half of the Nopah and Resting Springs Ranges, Nevada ad California *Geological Society of America Bulletin*, **94**, 1359-1376.

Carter, J., Taylor, W. J., and Luke, B. (2008). Structural and Sedimentological Development of Pahrump Basin, Southern Nevada with Implications for Seismic Hazards *EOS Transactions*, 53, **89**.

Cooper, J. D., Miller, R. H., and Sundberg, F. A. (1982). Environmental Stratigraphy of the Lower Part of the Nopah Formation (Upper Cambrian), Southwestern Great Basin, *Geology of Selected Areas in San Bernardino Mountains, Western Mojave Desert, and Southern Great Basin, California (Guidebook)*, Cooper, J. D., Troxel, B. W., and Wright, L. A., Geological Society of America, Anaheim, 97-116.

de Polo, C. (2003). *Preliminary Geologic Map of the Northeast Quarter of the Stewart Valley Quadrangle, Nye County, Nevada, and Inyo County, California*: Nevada, Nevada Bureau of Mines and Geology.

Dokka, R. K. and Travis, C. J. (1990). Late Cenozoic Strike-Slip Faulting in the Mojave Desert, California *Tectonics*, 2, **9**, 311-340.

Dokka, R. K. and Travis, C. J. (1990). Role of the Eastern California Shear Zone in Accomodating Pacific-North American Plate Motion *Geophysical Research Letters*, 9, **17**, 1323-1326.

Frankel, K. L., Dolan, J. F., Finkel, R. C., Owen, L. A., and Hoeft, J. S. (2007). Spatial variations in slip rate along the Death Valley-Fish Lake Valley fault system determined from LiDAR topographic data and cosmogenic 10Be geochronology *Geophysical Research Letters*, L18303, **34**.

Guest, B., Niemi, N., and Wernicke, B. (2007). Stateline Fault System: A New Component of the Miocene-Quaternary Eastern California Shear Zone *GSA Bulletin*, 11/12, **119**, 1337-1346.

Hill, E. M. and Blewitt, G. (2006). Testing for Fault Activity at Yucca Mountain, Nevada, Using Independent GPS Results From the BARGEN Network *Geophysical Research Letters*, LI4302, **33**.

Hoffard, J. L. (1991). *Quaternary Tectonics and Basin History of Pahrump and Stewart Valleys, Nevada and California*, masters thesis: University of Nevada, Reno, 157.

Kirby, E., Anandakrishnan, S., Phillips, F., and Marrero, S. (2008). Late Pleistocene slip rate along the Owens Valley fault, eastern California *Geophysical Research Letters*, L01304, **35**.

Louie, J., Shields, G., Ichinose, G., Hasting, M., Plank, G., and Bowman, S., (1998). Shallow Geophysical Constraints on Displacement and Segmentation of the Pahrump Valley Fault Zone, California-Nevada Border,Proceedings of the Basin and Range Province Seismic Hazards Summit.

McCalpin, J. P. (1996). *Paleoseismology*, Academic Press, San Diego, CA, 588.

Menges, C. M., Fridrich, C., Blakely, R. J., and Thompson, R. A. (2003). Late Quaternary Surface Rupture and Associated Transpressive Uplift on a Section of teh State Line Fault in South-Central Amargosa Desert Basin, Southwestern Nevada *EOS Trans.*, **84**, S11D-0327.

Morrison, R. B. (1991). Quaternary stratigraphic, hydrologic, and climatic history of the Great Basin, with emphasis on Lakes Lahontan, Bonneville, and Tecopa, *Quaternary Nonglacial Geology: Conterminous U.S.*, Morrison, R. B., Geological Society of America, Boulder, CO, 283-320.

Neimi, N., Guest, B., and Wernicke, B. (2005). Geomorphic Expression and Neotectonic Evaluation of a Diffuse Fault System from Airborne Laser Swath Mapping, Pahrump Valley, California and Nevada *EOS Trans*, 52, **86**, Fall Meeting Supplemental, Abstract H34B-02.

Oskin, M. and Iriondo, A. (2004). Large-Magnitude Transient Strain Accumulation on the Blackwater Fault, Eastern California Shear Zone *Geology*, 4, **32**, 313-316.

Piety, L. A. (1996). *Compilation of Known or Suspected Quaternary Faults Within 100 km of Yucca Mountain*, U.S. Geological Survey, OFR 94-0112

Poole, F. G. and Sandberg, C. A. (1977). Mississippian Paleogeography and Tectonics of the Western United Stats, *Paleozoic Paleogeography of the Western United States*, Stewart, J. H., Stevens, C. H., and Fritsche, A. E., Pacific Section, Society of Economic Paleontologists and Mineralogists, Pacific Coast Paleogeography Symposium 1.

Savage, J. C., Lisowski, M., and Prescott, W. H. (1990). An Apparent Shear Zone Trending North-Northwest Across the Mojave Desert Into Owens Valley, Eastern California *Geophysical Research Letters*, 12, **17**, p. 2113-2116.

Schweickert, R. A. and Lahren, M. M. (1997). Strike-Slip Fault System in Amargosa Valley and Yucca Mountain, Nevada *Tectonophysics*, 272, 25-41.

Sheriff, R. E. (1975). Factors Affecting Seismic Amplitudes *Geophysical Prospecting*, 23, 125-138.

Shields, G., Kip, A., Brigham, R., Crosbie, R., Trimble, L., Sleeman, M., Tucker, R., Zhan, H., and Louie, J. N. (1998). Shallow Geophysical Survey Across the Pahrump Valley Fault Zone, California-Nevada Border *Geological Society of America Bulletin*, 1, **88**, 270-275.

Snow, J. K. and Wernicke, B. (2000). Cenozoic Tectonism in the Central Basin and Range; Magnitude, Rate and Distribution of the Upper Crustal Strain *American Journal of Science*, **300**, 659-719.

Stevens, C. H. (1991). Paleogeographic and Structural Significance of an Upper Mississippian Facies Boundary in Southern Nevada and East-Central California *Geological Society of America Bulletin*, **vol. 103**, p. 875-885.

Stewart, J. H., Albers, J. P., and Poole, F. G. (1968). Summary of Regional Evidence for Right-Lateral Displacement in the Western Great Basin *Geological Society of America Bulletin*, **vol. 79**, p. 1407-1413.

Walker, J. D., Burchfiel, B. C., and Davis, G. A. (1995). New Age Controls on Initiation and Timing of the Forland Belt Thrusting in the Clark Mountains, Southern California *Geological Society of America Bulletin*, **vol. 107**, p. 742-750.

Wernicke, B. P. (1992). Cenozoic Extensional Tectonics of the U.S. Cordillera, *The Cordilleran Orogen: Conterminous U. S.*, Burchfiel, B. C., Lipman, P. W., and Zoback, M. L., Geological Society of America, Boulder, Colorado, 553-581.

Wernicke, B. P., Davis, J. L., Bennett, R. A., Normandeau, J. E., Friedrich, A. M., and Niemi, N. A. (2004). Tectonic Implications of a Dense Continuous GPS Velocity Field at Yucca Mountain, Nevada *Journal of Geophysical Research*, B12404, **109**, 13.

APPENDIX A CMP STACKS FOR LINES 6 AND 7

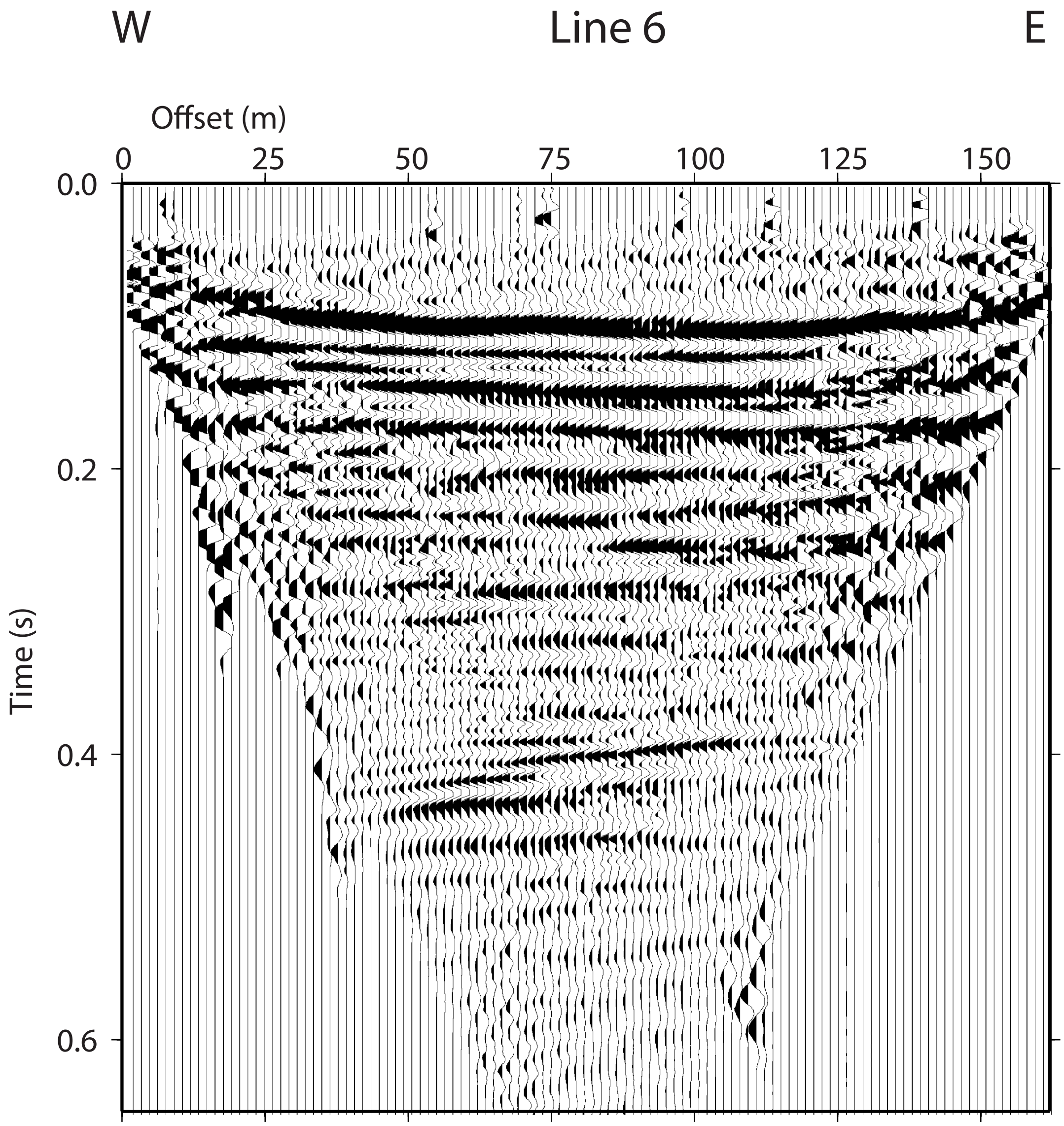

Uninterpreted, unmigrated CMP Stack for Line 6 (Figure 3). This profile was collected south of Line 1 and was 177 m in length.

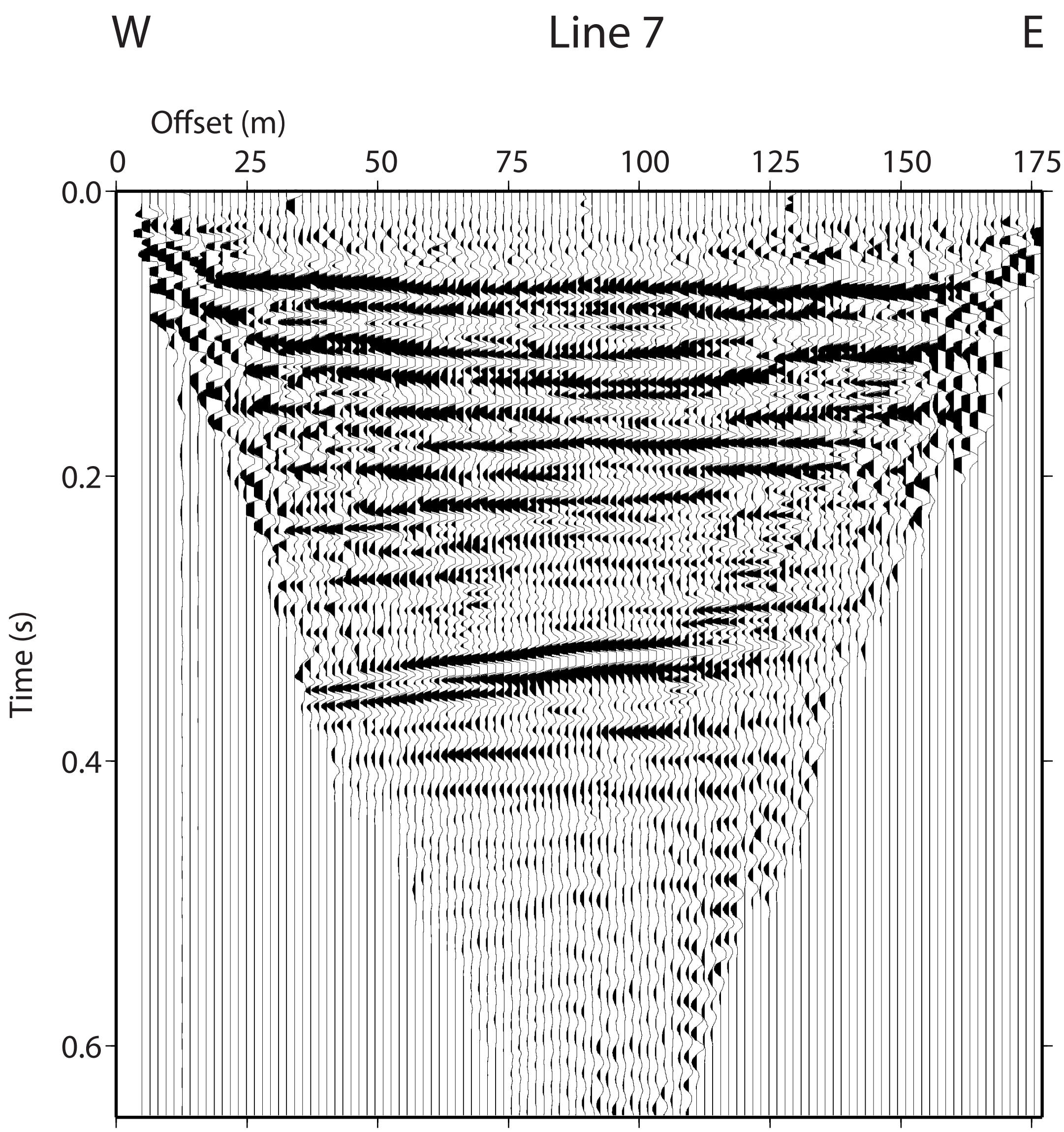

Uninterpreted, unmigrated CMP Stack for Line 7 (Figure 3). This profile was collected along a portion of Line 4 and is 176 m in length.

APPENDIX B VELOCITY TABLES

	Line 1	
TWTT (ms)	Velocity (m/s)	Depth (m)
0	1164.37	0.00
16.13	1164.37	9.39
32.26	1164.37	18.78
48.39	1170.32	28.22
64.52	1192.13	37.83
80.65	1213.38	47.62
96.77	1234.14	57.57
112.9	1254.57	67.69
129.03	1274.89	77.97
145.16	1295.36	88.41
161.29	1316.29	99.03
177.42	1337.91	109.82
193.55	1360.48	120.79
209.68	1384.11	131.96
225.81	1408.91	143.32
241.94	1434.8	154.89
258.06	1461.69	166.67
274.19	1489.27	178.68
290.32	1517.14	190.92
306.45	1544.95	203.38
322.58	1572.23	216.06
338.71	1598.43	228.95
354.84	1623.11	242.04
370.97	1646.15	255.32
387.1	1664.96	268.74
403.23	1664.96	282.17
419.35	1664.96	295.59
435.48	1664.96	309.02
451.61	1664.96	322.45
467.74	1664.96	335.88
483.87	1664.96	349.30
500	1664.96	362.73
516.13	1664.96	376.16
532.26	1664.96	389.59
548.39	1664.96	403.01
564.52	1664.96	416.44
580.65	1664.96	429.87
596.77	1664.96	443.29
612.9	1664.96	456.72
629.03	1664.96	470.15
645.16	1664.96	483.57
661.29	1664.96	497.00

Line 2

TWTT (ms)	Velocity (m/s)	Depth (m)
0	1208	0.00
13.16	1208	7.95
26.32	1208	15.90
39.47	1208	23.84
52.63	1208	31.79
65.79	1208	39.74
78.95	1208	47.69
92.11	1248.81	55.90
105.26	1261.98	64.20
118.42	1276.89	72.60
131.58	1293.43	81.11
144.74	1311.25	89.74
157.89	1329.99	98.49
171.05	1349.24	107.36
184.21	1368.63	116.37
197.37	1387.88	125.50
210.53	1406.79	134.76
223.68	1425.2	144.13
236.84	1443.06	153.62
250	1460.32	163.23
263.16	1476.97	172.95
276.32	1493.02	182.78
289.47	1508.49	192.69
302.63	1523.42	202.72
315.79	1537.84	212.84
328.95	1551.81	223.05
342.11	1565.37	233.35
355.26	1578.56	243.73
368.42	1591.44	254.20
381.58	1604.04	264.75
394.74	1616.42	275.39
407.89	1628.61	286.10
421.05	1640.65	296.89
434.21	1652.57	307.77
447.37	1664.41	318.72
460.53	1676.18	329.75
473.68	1687.92	340.85
486.84	1699.64	352.03
500	1711.36	363.29
513.16	1723.09	374.63
526.32	1734.85	386.04
539.47	1746.64	397.53
552.63	1758.46	409.10
565.79	1770.34	420.75
578.95	1782.26	432.47
592.11	1788.69	444.24
605.26	1788.69	456.01
618.42	1788.69	467.77
631.58	1788.69	479.54

Line 2		
TWTT (ms)	Velocity (m/s)	Depth (m)
644.74	1788.69	491.31

	Line 3	
TWTT (ms)	Velocity (m/s)	Depth (m)
0	1292.93	0.00
11.36	1292.93	7.34
22.73	1292.93	14.69
34.09	1292.93	22.04
45.45	1292.93	29.38
56.82	1322.81	36.90
68.18	1358.69	44.62
79.55	1393.06	52.54
90.91	1422.39	60.62
102.27	1442.32	68.81
113.64	1454.55	77.08
125	1462.19	85.38
136.36	1467.78	93.72
147.73	1473.75	102.10
159.09	1480.26	110.51
170.45	1489.78	118.97
181.82	1503.53	127.52
193.18	1521.37	136.16
204.55	1542.02	144.93
215.91	1563.69	153.81
227.27	1584.21	162.81
238.64	1602.29	171.91
250	1617.37	181.10
261.36	1629.76	190.36
272.73	1640.3	199.68
284.09	1649.82	209.05
295.45	1659.01	218.48
306.82	1660.69	227.92
318.18	1660.69	237.35
329.55	1660.69	246.79
340.91	1660.69	256.22
352.27	1660.69	265.66
363.64	1660.69	275.10
375	1660.69	284.53
386.36	1660.69	293.96
397.73	1660.69	303.40
409.09	1660.69	312.84
420.45	1660.69	322.27
431.82	1660.69	331.71
443.18	1660.69	341.14
454.55	1660.69	350.59
465.91	1660.69	360.02
477.27	1660.69	369.45
488.64	1660.69	378.89
500	1660.69	388.32
511.36	1660.69	397.76
522.73	1660.69	407.20
534.09	1660.69	416.63
545.45	1660.69	426.06

Line 3		
TWTT (ms)	Velocity (m/s)	Depth (m)
556.82	1660.69	435.50
568.18	1660.69	444.94
579.55	1660.69	454.38
590.91	1660.69	463.81
602.27	1660.69	473.24
613.64	1660.69	482.68
625	1660.69	492.12
636.36	1660.69	501.55
647.73	1660.69	510.99

Line 4

TWTT (ms)	Velocity (m/s)	Depth (m)
0	1235.37	0.00
10.99	1235.37	6.79
21.98	1235.37	13.58
32.97	1235.37	20.37
43.96	1235.37	27.15
54.95	1235.37	33.94
65.93	1235.37	40.72
76.92	1235.37	47.51
87.91	1235.37	54.30
98.9	1235.37	61.09
109.89	1235.37	67.88
120.88	1235.37	74.67
131.87	1235.37	81.45
142.86	1235.37	88.24
153.85	1235.37	95.03
164.84	1235.37	101.82
175.82	1238.53	108.62
186.81	1249.29	115.48
197.8	1260.68	122.41
208.79	1272.64	129.40
219.78	1285.1	136.47
230.77	1298.01	143.60
241.76	1311.28	150.80
252.75	1324.82	158.08
263.74	1338.57	165.44
274.73	1352.45	172.87
285.71	1366.43	180.37
296.7	1380.49	187.96
307.69	1394.59	195.62
318.68	1408.72	203.36
329.67	1422.84	211.18
340.66	1436.92	219.08
351.65	1450.93	227.05
362.64	1464.86	235.10
373.63	1478.71	243.22
384.62	1492.47	251.43
395.6	1505.06	259.69
406.59	1505.06	267.96
417.58	1505.06	276.23
428.57	1505.06	284.50
439.56	1505.06	292.77
450.55	1505.06	301.04
461.54	1505.06	309.31
472.53	1505.06	317.58
483.52	1505.06	325.85
494.51	1505.06	334.12
505.49	1505.06	342.38
516.48	1505.06	350.65
527.47	1505.06	358.92

Line 4

TWTT (ms)	Velocity (m/s)	Depth (m)
538.46	1505.06	367.20
549.45	1505.06	375.47
560.44	1505.06	383.74
571.43	1505.06	392.01
582.42	1505.06	400.28
593.41	1505.06	408.55
604.4	1505.06	416.82
615.38	1505.06	425.08
626.37	1505.06	433.35
637.36	1505.06	441.62
648.35	1505.06	449.89

Line 5

TWTT (ms)	Velocity (m/s)	Depth (m)
0	1063.37	0.00
23.26	1063.37	12.37
34.88	1063.37	18.55
46.51	1063.37	24.73
58.14	1063.37	30.91
69.77	1063.37	37.10
81.4	1069.11	43.31
93.02	1082.44	49.60
104.65	1096.19	55.98
116.28	1110.33	62.43
127.91	1124.8	68.97
139.53	1139.54	75.59
151.16	1154.44	82.31
162.79	1169.44	89.11
174.42	1184.49	96.00
186.05	1199.54	102.97
197.67	1214.55	110.03
209.3	1229.5	117.18
220.93	1244.39	124.41
232.56	1259.21	131.73
244.19	1273.96	139.14
255.81	1288.66	146.63
267.44	1303.32	154.21
279.07	1317.94	161.87
290.7	1332.53	169.62
302.33	1347.1	177.45
313.95	1361.65	185.37
325.58	1376.18	193.37
337.21	1390.7	201.46
348.84	1405.2	209.63
360.47	1419.69	217.88
372.09	1434.17	226.21
383.72	1448.63	234.64
395.35	1463.08	243.15
406.98	1477.53	251.74
418.6	1491.96	260.41
430.23	1506.38	269.17
441.86	1514.52	277.97
453.49	1514.52	286.78
465.12	1514.52	295.59
476.74	1514.52	304.39
488.37	1514.52	313.19
500	1514.52	322.00
511.63	1514.52	330.81
523.26	1514.52	339.61
534.88	1514.52	348.41
546.51	1514.52	357.22
558.14	1514.52	366.03
569.77	1514.52	374.83

Line 5

TWTT (ms)	Velocity (m/s)	Depth (m)
581.4	1514.52	383.64
593.02	1514.52	392.44
604.65	1514.52	401.25
616.28	1514.52	410.05
627.91	1514.52	418.86
639.53	1514.52	427.66
651.16	1514.52	436.47

Line 6

TWTT (ms)	Velocity (m/s)	Depth (m)
0	1298.14	0
20.41	1298.14	13.25
40.82	1298.14	26.50
61.22	1298.14	39.74
81.63	1298.14	52.98
102.04	1312.2	66.37
122.45	1326.67	79.91
142.86	1341.05	93.60
163.27	1355.37	107.43
183.67	1369.64	121.40
204.08	1383.89	135.52
224.49	1398.16	149.79
244.9	1412.44	164.21
265.31	1426.7	178.76
285.71	1440.91	193.46
306.12	1455.07	208.31
326.53	1469.2	223.30
346.94	1483.31	238.44
367.35	1497.45	253.72
387.76	1511.61	269.15
408.16	1511.92	284.57
428.57	1511.92	300.00
448.98	1511.92	315.43
469.39	1511.92	330.86
489.8	1511.92	346.29
510.2	1511.92	361.71
530.61	1511.92	377.14
551.02	1511.92	392.57
571.43	1511.92	408.00
591.84	1511.92	423.43
612.24	1511.92	438.85
632.65	1511.92	454.28
653.06	1511.92	469.71

Line 7

TWTT (ms)	Velocity (m/s)	Depth (m)
0	1417.42	0
15.38	1417.42	10.90
30.77	1417.42	21.81
46.15	1417.42	32.71
61.54	1417.42	43.61
76.92	1417.42	54.51
92.31	1421.36	65.45
107.69	1425.6	76.41
123.08	1429.76	87.42
138.46	1434.01	98.44
153.85	1438.46	109.51
169.23	1443.11	120.61
184.62	1447.82	131.75
200	1452.53	142.92
215.38	1457.36	154.13
230.77	1462.42	165.38
246.15	1467.67	176.67
261.54	1473	188.00
276.92	1478.36	199.37
292.31	1483.8	210.79
307.69	1489.37	222.24
323.08	1495.03	233.75
338.46	1500.75	245.29
353.85	1506.49	256.88
369.23	1512.27	268.51
384.62	1518.09	280.19
400	1523.94	291.91
415.38	1529.8	303.67
430.77	1530.01	315.45
446.15	1530.01	327.21
461.54	1530.01	338.99
476.92	1530.01	350.75
492.31	1530.01	362.53
507.69	1530.01	374.29
523.08	1530.01	386.07
538.46	1530.01	397.83
553.85	1530.01	409.60
569.23	1530.01	421.37
584.62	1530.01	433.14
600	1530.01	444.91
615.38	1530.01	456.68
630.77	1530.01	468.45
646.15	1530.01	480.21